Comprehensive Topographical Map of the Serotonergic Fibers in the Mouse Brain

Janak R. Awasthi[1,2], Kota Tamada[1], Eric T. N. Overton[1], Toru Takumi[1,2,3*]

[1]RIKEN Brain Science Institute, Wako, Saitama 351-0198, Japan

[2]Graduate School of Science and Engineering, Saitama University, Sakura, Saitama 338-8570, Japan

[3]Department of Physiology and Cell Biology, Kobe University School of Medicine, Chuo, Kobe 650-0017, Japan

***Correspondence to:**

Toru Takumi

RIKEN Center for Brain Science, 2-1 Hirosawa, Wako, Saitama 351-0198, Japan.

TEL: +81 48 467 5906, FAX: +81 48 467 6079

Email: toru.takumi@riken.jp

Funding information

This work was supported partly by KAKENHI (16H06316, 16H06463) from Japan Society for the Promotion of Science and Ministry of Education, Culture, Sports, Science, and Technology, Intramural Research Grant for Neurological and Psychiatric Disorders of NCNP, the Takeda Science Foundation and Smoking Research Foundation. Awasthi has been awarded the International Program Associate (IPA) fellowship from the RIKEN - Saitama University joint frontier program, Japan.

Abstract

It is well established that serotonergic fibers distribute throughout the brain. Abnormal densities or patterns of serotonergic fibers have been implicated in neuropsychiatric disorders. Although many classical studies have examined the distribution pattern of serotonergic fibers, most of them were either limited to specific brain areas or had limitations in demonstrating the fine axonal morphology. In this study, we utilize transgenic mice expressing GFP under the SERT promoter to map the topography of serotonergic fibers across the rostro-caudal extent of each brain area. We demonstrate previously unreported regional density and fine-grained anatomy of serotonergic fibers. Our findings include: 1) SERT fibers distribute abundantly in the thalamic nuclei close to the midline and dorsolateral areas, in most of the hypothalamic nuclei with few exceptions such as the median eminence and arcuate nuclei, and within the basal amygdaloid complex and lateral septal nuclei, 2) the source fibers of innervation of the hippocampus traverse through the septal nuclei before reaching its destination, 3) unique, filamentous type of straight terminal fibers within the nucleus accumbens, 4) laminar pattern of innervation in the hippocampus, olfactory bulb and cortex with heterogenicity in innervation density among the layers, 5) cortical labelling density gradually decreases rostro-caudally, 6) fibers traverse and distribute mostly within the gray matter, leaving the white fiber bundles uninnervated, and 7) most of the highly labelled nuclei and cortical areas have predominant anatomical connection to limbic structures. In conclusion, we provide novel, regionally specific insights on the distribution map of serotonergic fibers using transgenic mouse.

Keywords: Serotonin, SERT, transgenic mouse, whole brain mapping

1. INTRODUCTION

Serotonin (5-hydroxytryptamine or 5-HT) is a well-recognized modulator of brain activity and other functions in peripheral organs (Berger et al., 2009). Dysfunction of 5-HT system has been implicated in mood disorders, schizophrenia, addiction, attention deficit hyperactivity disorder, autism spectrum disorders (ASD) and other mental disorders (Lin et al., 2014). In fact, results of several biological studies demonstrate alterations of morphology and/or density of 5-HT neurons in several mental disorders such as depression (Rajkowska et al., 2017), ASD (Makkonen et al., 2008) (Tamada and Takumi, 2015), schizophrenia (Hrovatin et al., 2019), traumatic brain injury (Abe et al., 2016) and in cases like prenatal exposure of psychotropic drugs (Xu et al., 2004) (Maciag et al., 2006) (Weaver et al., 2010), neonatal hypoxia (Reinebrant et al., 2020), or postnatal social isolation (Kuramochi and Nakamura, 2009).

The 5-HT fibers originate from discretely organized cell somas in the raphe nuclei of brainstem and project throughout the brain (Fuxe, 1965) (Vertes and Linley, 2008). In parallel, the activities of these raphe cell bodies are regulated by the monosynaptic inputs from the forebrain and brainstem neurons (Pollak Dorocic et al., 2014). A total of 28,000 5-HT producing neurons in the mouse brain (Ishimura et al., 1988) does not act as a single population, but rather contains parallel sub-systems that differ in connectivity, physiological properties, and behavioral functions (Ren et al., 2018) (Okaty et al., 2019). Its diversity is additionally exhibited by recent transcriptomics study suggesting that the dorsal raphe (DR) 5-HT neurons co-expressing Vglut-3 preferentially innervate the cortex, whereas those co-expressing thyrotropin-releasing hormones innervate the subcortical regions (Ren et al., 2019). The anterograde tracing approaches have revealed that serotonergic efferents from different raphe nuclei to the major brain regions are distinctive and largely non-overlapping (Muzerelle et al., 2016). Although these recent dissections of serotonergic system have unearthed its much finer

details, the precise and comprehensive topographical map of total 5-HT efferents in whole brain remains undetermined by the recent neuroanatomical tools.

The serotonergic topography has long been studied with the progressive advent of neuroanatomical techniques such as aldehyde histofluorescence (Fuxe, 1965), autoradiography (Parent et al., 1981), immunohistochemical techniques using antibodies against 5-HT marker enzyme tryptophan hydroxylase (Tph) (Pickel et al., 1977) or 5-HT itself (Steinbusch, 1981). However, they were accompanied by several limitations: These techniques neither allowed the unambiguous identification of labelled 5-HT or non-5-HT neurons, nor were they ideal for visualizing the fine terminal axons due to either the dilution of tracer in highly ramified axons (Parent et al., 1981) or rapid metabolization of released 5-HT, requiring pretreatment before tissue harvesting (Azmitia and Gannon, 1983). Moreover, the synthesis rate or metabolism of 5-HT or Tph, which is subjected to large variability depending on the environmental conditions, may contribute to the alteration in the staining outcome (Nielsen et al., 2006). Therefore, the actual picture of 5-HT innervation in the brain must be more extensive than that revealed by these techniques.

To ensure high fidelity visualization of the fine-grain anatomy of the serotonergic system, we employed SERT (serotonin transporter) -EGFP (enhanced green fluorescence protein) bacterial artificial chromosome (BAC) transgenic mouse in which an EGFP reporter gene is inserted upstream of the coding sequence of the SERT gene (Schmidt et al., 2013). Combined with GFP antibody and high-resolution imaging, we present better organization of serotonergic fibers with the complete visualization of the whole axons, their morphological features and distribution across the whole brain of the adult mice.

2. MATERIAL AND METHODS

2.1 Animals

All procedures for animal experiments were carried out in accordance with the guidelines of the animal experimentation committee of RIKEN, Japan. The mouse strain used for this research was STOCK Tg (Slc6a4-EGFP) JP55Gsat/Mmucd (RRID: MMRRC_030692-UCD) which was obtained from Research Resources Division, RIKEN. Originally, the mice were obtained from the Mutant Mouse Resource and Research Center (MMRRC) at University of California at Davis, a NIH-funded strain repository, and was donated to the MMRRC by Nathaniel Heintz, The Rockefeller University (Gong et al., 2003). The mice line was maintained by mating male *SERT-EGFP* mice with wild type female C57BL/6J mice (backcrossed more than 5 times). All mice were maintained on a 12/12-hour light/dark cycle and housed in standard plexiglass cages with food and water ad libitum.

2.2 Immunohistochemistry

Eleven-week-old male mice (*n*=4) were anesthetized and transcardially perfused with phosphate buffer saline (PBS) followed by 4% paraformaldehyde (PFA) in 0.1 M phosphate buffer (pH 7.4). Brains were removed and immersion-fixed with 4% PFA at 4°C overnight. Coronal (100 µm thick) and sagittal (60 µm thick) sections were made using Leica VT1200 S vibratome (Leica Microsystems, Nussloch, Germany) and collected in PBS containing 0.01% sodium azide and stored at 4°C until use. Immunohistochemical procedures were performed on free floating sections. Sections were treated with 0.3% H_2O_2 in PBS for 30 minutes, washed with PBS for 5 minutes three times, incubated with a blocking solution (PBS containing 3% normal goat serum and 0.3% Triton X-100) for 30 minutes at room temperature, and incubated with primary antibodies [Anti GFP rabbit polyclonal antibody (1:500 dilution; #catalog no: A-11122, Thermo Fisher Scientific, Tokyo, Japan)] diluted with the blocking solution overnight at 4°C. Sections were washed with PBS containing 0.3% Triton X-100 (PBST) for 10 minutes four times, incubated with fluorescent-conjugated secondary antibodies [Alexa Fluor 488 Goat anti-Rabbit IgG (1:500 dilution; catalog # A-11034; Thermo Fisher Scientific, Tokyo, Japan)]

diluted with the blocking solution for 2 hours at room temperature, washed with PBST for 10 minutes four times, transferred onto Superfrost slides, and mounted with VECTASHIELD with DAPI (Vector Laboratories, Burlingame, CA, USA)

2.3 Images acquisition and analysis

The sections were imaged at 10X magnification with VS120 (Olympus, Tokyo, Japan) whole slide scanner fluorescent microscope and FV3000 confocal microscope (Olympus, Tokyo, Japan). The images were processed using ImageJ (Rasband, 1997) and Adobe photoshop CS6, and were converted into grayscale and adjusted for brightness and contrast. Finally, the borders were manually drawn around the nuclei using Inkscape software (Harrington, 2005) upon comparing the SERT immunolabelled sections with its DAPI stained counterparts with the aid of the Allen brain atlas (Allen Institute for Brain Science, 2004). The density of serotonergic fibers in each nucleus was then rated on a scale of 0 to 6 (Table 1).

Table 1 Fiber density ratings

Density rating	Description	Definition
0	Scanty	lowest density of fibers; more background than fibers
1	Sparse	low, more background than fibers
2	Mild	slightly more background than fibers
3	Moderate	balance between fibers and background
4	Moderately high	more fibers than background
5	Dense	possible to distinguish individual fibers
6	Very dense	highest density of fibers; difficult to distinguish individual fibers

The representative image for each scale is depicted in supplementary figure 1.

3. RESULTS

In this study, we comprehensively mapped the distribution pattern of the serotonergic fibers across the rostro-caudal extent of each brain regions and sub-regions using the SERT-EGFP transgenic mice that was genetically modified to express GFP in the serotonergic fibers. The serotonergic fibers arising from the discrete clusters of cell bodies in the midbrain raphe nuclei innervated nearly all the brain areas in a specific pattern and innervation density. The study

plan and the results are depicted schematically in supplementary figure 2. In the following account, we describe the projection pattern and rostro-caudal density gradient in each nucleus of various brain areas and their sub-divisions.

3.1 INNERVATION PATTERN IN THE THALAMUS

We analyzed the innervation density and the pattern of SERT-EGFP fibers across the rostro-caudal extent of different thalamic nuclei. No thalamic nuclei were devoid of the innervation. In order to ease the description, we categorized the thalamic nuclei according to the recent classification concept viz; (1) midline and intralaminar nuclei (2) association nuclei (3) principal nuclei (4) epithalamus and (5) the reticular nucleus (Groenewegen and Witter, 2004). Towards the rostral pole of the thalamus, we observed that some of the dorsally diverted collaterals of pathway fibers from the lateral preoptic area (LPO) and lateral hypothalamic area (LHA) passed around the column of fornix and/or along the zona incerta (ZI) to project into the ventrally located thalamic nuclei such as the nucleus reuniens (RE) (Figure 1B & 2C, arrow). Meanwhile, towards the caudal thalamic levels, we noticed that laterally directed collaterals of pathway fibers passed across the ZI to innervate the lateral geniculate (LG) nuclei (Figure 1G). Similarly, rostrally directed collaterals of pathway fibers from the periaqueductal gray (PAG) (Figure 1G), which traversed through the paraventricular thalamic nuclei (PVT) (Figure 1E, arrow), provided the innervation to the dorsally located thalamic nuclei of caudal pole (ex; PVT and other neighboring nuclei).

3.1.1 Midline nuclei

The midline nuclei include paraventricular thalamic (PVT), paratenial (PT), rhomboid (RH) nuclei and nucleus reuniens (RE). We observed that the entire anteroposterior axis of these nuclei was very densely (6+) labeled with a couple of exceptions. For example, the labeling density within RH nuclei decreased to moderate (3+) density at its caudal extent (Figure 1E), while the PT nucleus was densely (5+) labeled (Figure 1A). We found that the ascending

pathway fibers traversing ahead from PAG were clustered as two bilateral bundles within the caudal PVT (Figure 1E, arrow) which diffused rostrally to innervate the other adjacent nuclei. There were other nuclei such as the intermediodorsal (IMD), interanteromedial (IAM), and interanterodorsal (IAD), which were located in the midline but were not considered part of the midline nuclei.

3.1.2 Intralaminar nuclei

These nuclei were anatomically associated with the medullary lamina of thalamus, thus were considered as a separate category despite their location in the thalamic midline. It consists of central lateral (CL), paracentral (PC), central medial (CM) and parafascicular (PF) nuclei (Groenewegen and Witter, 2004). We observed that SERT-EGFP fiber density within the CM nuclei gradually decreased from very dense (6+) labelling (Figure 1A) to sparse (1+) density (Figure 1D), and progressively became milder (2+) towards its caudal extent (Figure 1F). We also noticed an intranuclear gradient at its caudal extent (Figure 1F). Similarly, we found that labelling density within CL nuclei gradually decreased from dense (5+) (Figure 1C) to sparse (1+) (Figure 1E) rostro-caudally. Likewise, innervation density within PC nuclei changed from moderate (3+) (Figure 1C) to scanty (0) level (Figure 1E) along the rostro-caudal extent, whereas PF nuclei exhibited intranuclear gradient with milder (2+) density on its dorsal aspect and sparse (1+) ventrally (Figure 1F).

3.1.3 Association nuclei

According to the aforementioned classification, thalamic association nuclei include the anterior nuclei and its subdivisions [anteroventral (AV), anterodorsal (AD), anteromedial (AM), interanteromedial (IAM)], lateral dorsal (LD), lateral posterior (LP), mediodorsal (MD), intermediodorsal (IMD) and submedial thalamic (SMT) nuclei. Among the different subdivisions of the anterior nuclei, we observed that AV nuclei were densely (5+) labelled throughout the rostro-caudal extent (Figure 1A-C). Similarly, AD nuclei received moderately

high (4+) projections (Figure 1A-B). AM and IAD nuclei had milder (2+) projections (Figure 1B), whereas the labelling density within IAM nuclei decreased from moderately high (4+) (Figure 1B) to milder (2+) density (Figure 1C) rostro-caudally. We spotted that LD (Figure 1B-E) and LP (Figure 1E-F) nuclei were densely (5+) labeled with slight decrease in their labelling density towards their caudal extent. The density of fibers within the MD nuclei decreased from moderate (3+) to mild (2+) one rostro-caudally (Figure 1 C-E). However, it exhibited higher labelling within the central (c) part compared to its medial (m) and lateral (l) area (Figure 1C-D). Similarly, the innervation density within IMD nuclei decreased from dense (5+) (Figure 1C) to moderate (3+) labelling (Figure 1F) along the rostro-caudal axis. Interestingly, the fiber density within the submedial nucleus exhibited distinct rostral–caudal gradient being moderately (3+) labeled at the rostral half (Figure 1B), sparsely (1+) at the intermediate level (Figure 1C) and its caudal extent was very densely (6+) labelled (Figure 1D-E).

3.1.4 Principal nuclei

Principal nuclei include the ventrobasal (VB) complex [ventral posteromedial (VPM) and ventral posterolateral nuclei (VPL)], ventroanterior lateral complex (VAL), ventromedial nucleus (VM), posterior nucleus (PO), the lateral (LG) and medial geniculate (MG) nuclei (Groenewegen and Witter, 2004). We noticed that the VB, VAL complexes, VM, and PO nuclei received almost no innervation (<1) (Figure 1D-F) except the PO nucleus at its rostral extent, which was sparsely (1+) labelled (Figure 1D). The LG nuclei complex was very densely (6+) innervated throughout the rostro-caudal extent (Figure 1E-G). However, the medial area of the ventral LG nuclei (LGv) had comparably less innervation (Figure 1F). Similarly, we noticed that MG nuclei were mildly (2+) labeled only on its lateral area (Figure 1G), thus showing the intranuclear gradient. We observed that the fascicles of SERT-EGFP fibers arising

from the PAG passed laterally along ZI to enrich the innervation of MG and LG nuclei (Figure 1G).

3.1.5 Medial and lateral habenula (epithalamus)

We found that the habenula was less innervated compared to other dorsally located thalamic nuclei. Medial habenula were sparsely (1+) labelled towards the rostral pole (Figure 1B). As traced caudally, the whole area of lateral habenula and only the lateral part of the medial habenula were moderately (3+) labelled (Figure 1C-D). This pattern was due to the collaterals of pathway fibers ascending ahead through the PVT being directed laterally along the borders in-between the medial and lateral habenula. The labelling density within the lateral habenula was moderately high (4+) towards the caudal extent (Figure 1F). Overall, the lateral habenula was innervated in higher density compared to the medial habenula.

3.1.6 Reticular nucleus

Except the moderately (3+) labelled rostral pole of reticular nuclei (Figure 1A), the rest of its extension received sparse (1+) innervation (Figure B-F). However, the innervation density was slightly higher than adjacently located ventrobasal complex of the thalamus (Figure 1D).

3.1.7 Other areas

The white fiber bundles; viz. fasciculus retroflexus (fr), mamillotegmental tract (mmt), posterior commissure (pc), internal capsule (int) and cerebral peduncle (cpd) were devoid of the innervation. However, few SERT-EGFP fibers passed around the white fibers within the cerebral peduncle (Figure 1F) to reach the globus pallidus (GP). We observed the collaterals of pathway fibers travelling within the stria medullaris (sm) and stria terminalis (st). Within stria terminalis, the fibers were dispersed throughout the tract (Figure 6D). However, fibers were clustered only in the dorsal part of sm leaving the rest of the part being devoid of the innervation (Figure 1A, arrow head).

3.2 INNERVATION PATTERN IN THE HYPOTHALAMUS

We categorized hypothalamic nuclei according to a conventional classification method based on regional location, viz; preoptic region, supraoptic region, tuberal region and mammillary region (D. G. Stuart, 1962). Preoptic and supraoptic regions were located towards the rostral hypothalamic zone, and the tuberal region was situated in the middle hypothalamic zone, whereas the mamillary region was positioned in the caudal hypothalamic zone. We noticed that the hypothalamic nuclei were heterogeneously innervated.

3.2.1 Preoptic region (Figure 2A-B)

The ascending forebrain bundle traversed rostrally through lateral preoptic region (LPO). Few thin, punctate fibers of innervation were scattered in between the thick ascending pathway fibers. Some of the detached fibers from the main ascending bundle were clustered separately within the substantia innominata (SI). The median preoptic nucleus (MEPO) and rostral part of medial preoptic area (MPO) were densely (5+) innervated (Figure 2A). However, the labelling density in MPO decreased as traced caudally, exhibiting the intranuclear gradient. The fibers were distributed moderately high (4+) on its lateral area and moderately (3+) on its medial part. (Figure 2B). The anteroventral periventricular nuclei (AVPV) were mildly (2+) innervated (Figure 2A), whereas the medial preoptic nucleus (MPN) received moderately high (4+) projection (Figure 2B). The other non-principal hypothalamic nuclei present in the preoptic region; viz, magnocellular nuclei (MA) and nucleus of diagonal band (NDB) were densely (5+) innervated (Figure 2A), although the labelling density in MA decreased slightly as traced caudally (Figure 2B). We observed that the collaterals of pathway fibers which were clustered in SI diverted medially to run over the lower border of MA and NDB in the area adjoining to OT, to finally enter into the septal nuclei (Figure 2A, arrow).

3.2.2 Supraoptic region (Figure 2C-F)

The ascending forebrain bundle traversed rostrally through the lateral hypothalamic area (LHA) with few interspersed fibers of innervation. The collaterals of ascending bundle passed

dorsally into the thalamic RE (Figure 2C, arrow) and laterally into the ZI (Figure 2F). Some of the collaterals ran ventromedially through supraoptic commissure and retrochiasmatic nuclei (RCN) (Figure 2F, arrow) to project into the rostrally located suprachiasmatic nuclei (SCN) (Figure 2D). We found that the supraoptic nuclei (SO) (Figure 2C & F) and rostral part of RCN (Figure 2C) were moderately (3+) labelled. However, the labelling density of latter increased densely (5+) caudally (Figure 2F). Anterior hypothalamic nuclei (AHN) were densely (5+) innervated throughout the rostro-caudal extent. Interestingly, we noticed that SCN exhibited both intranuclear and rostro-caudal gradients. Rostral (Figure 2C) and caudal (Figure 2E) SCN was sparsely (1+) innervated. However, the intranuclear gradient was observed in midway SCN (Figure 2D). Its ventromedial area (core) received very dense (6+) projections making it one of the most heavily innervated brain areas while the dorsolateral area (shell) was sparsely (1+) innervated. Similarly, we observed rostro-caudal gradient in the sub-paraventricular zone (SBPV) in which innervation density increased from moderate (3+) (Figure 2C) to dense (5+) levels (Figure 2F). Paraventricular hypothalamic nuclei (PVH) exhibited both intranuclear and rostro-caudal gradients. Rostrally, except its densely (5+) innervated periventricular part (PVHpv) (Figure 2D), the rest of its area was sparsely (1+) labelled (Figure 2C-E). However, at its caudal extent the whole PVH nucleus was densely (5+) labelled (Figure 2F).

3.2.3 Tuberal region (Figure 2G-H)

The ascending forebrain bundle traversed rostrally through the perifornical LHA of tuberal region. The ventromedial hypothalamic nuclei (VMH) exhibited intranuclear gradient across the rostro-caudal axis. Rostrally, its dorsomedial (dm) part was mildly (2+) innervated compared to the rest of the nucleus (5+) (Figure 2G). However, the fibers were densely (5+) and homogeneously distributed throughout the nucleus as traced caudally (Figure 2H). Similarly, we noticed that the dorsomedial hypothalamic nuclei (DMH) were densely (5+) innervated rostrally (Figure 2G) and labelled mildly (2+) at its caudal extent (Figure 2H),

displaying the rostro-caudal gradient. The arcuate nucleus exhibited sparse labelling (1+) throughout the antero-posterior axis. We found that the collateral fibers arising from the main ascending bundle in LHA projected ventrally into the tuberal (TU) nuclei making it densely (5+) innervated.

3.2.4 Mamillary region (Figure 2I-K)

We observed that the innervation density within the posterior hypothalamic nuclei (PH) decreased from dense (5+) (Figure 2H-I) to sparse (1+) density (Figure 2K) rostro-caudally. Moreover, we noticed that PH nuclei served as the route for the collateral fibers (arising from the main ascending bundle in the LHA) to pass dorsally into the thalamus (Figure 2H). Similarly, the posterior part of periventricular nuclei (PVp) (Figure 2I-J) and supramamillary nuclei (SuM) (Figure 2J, 2K) had sparse (1+) labelling throughout the rostro-caudal extent. Likewise, the both ventral and dorsal parts of premamillary (PMv, PMd) nuclei were labelled in moderately high (4+) density (Figure 2I). We spotted collaterals arising from the ascending fiber bundle at VTA running directly into the lateral mamillary nuclei (LM) making it densely (5+) innervated (Figure 2J, arrow). Similarly, the ventral part of tuberomammillary (TMv) was labelled in moderately high (4+) density (Figure 2J), whereas the dorsal part being mildly (2+) innervated (Figure 2I). The median part of medial mamillary nuclei (MMme) was densely (5+) labelled, while the rest had innervation with slightly less density (4+) (Figure 2J). However, the pattern was in contrary to its caudal extent (Figure 2K). Strikingly, the median eminence had almost no SERT-EGFP labelled fibers (Figure 2H-I).

There were few nuclei which extended over more than one region and the patterns they exhibited were as follows: the mediolaterally extended nuclei ZI carried the collaterals of the main ascending bundle from LHA towards laterally located thalamic reticular nuclei or the geniculate nuclei (Figure 1E-G). We observed that the SERT-EGFP fiber distributed over ZI gradually decreased from the dense (5+) (Figure 2F) to sparse (1+) density (Figure 2I) rostro-

caudally. Subthalamic nuclei (STN) that were located just above the cerebral peduncle (cpd) were densely (5+) labelled because of the directly entering collaterals of ascending bundle fibers from LHA (Figure 2H-I). We noticed heterogenicity among the different subdivisions of periventricular nuclei (PV). The preoptic (PVpo) (Figure 2B), anterior (PVa) (Figure 2C), and intermediate (PVi) (Figure 2D) parts of PV nuclei were densely (5+) innervated. The AVPV and PVp nuclei with less innervation have been already included in the preoptic region and mamillary region, respectively.

3.2.5 Other areas within the hypothalamic zone

The optic tract (opt) was completely devoid of innervation (Figure 2F-G). However, some fibers which entered into the SCN received serotonergic innervation (Figure 2D, arrow head). The white fiber bundles, viz. fornix (fx) (Figure 2B)**,** mamillotegmental tract (mtt) (Figure 2H-I), anterior commissure (aco, act) (Figure 2A, B) and cerebral peduncle (cpd) (Figure 2 I-J) appeared almost empty with very few scattered fibers traversing along or through it.

3.3 INNERVATION PATTERN IN THE AMYGDALA

We observed that no nuclei within the amygdaloid complex were devoid of the serotonergic innervation. However, they exhibited heterogenicity in the innervation density and gradient along the rostro-caudal axis. We noticed that collaterals of pathway fibers entered into the amygdala via two routes, via the lateral hypothalamic area (LHA) / substantia innominata (SI) (Figure 3A, arrow) and via the stria terminalis (st) (Figure 3C-D). The fibers contained in stria terminalis originated from the main ascending bundle at lateral preoptic area (LPO) (Figure 6D) and ran caudally over the thalamus to ultimately project to the amygdalar nuclei (Figure 3C, D). These collaterals of pathway fibers were scattered among the thin and punctate fibers of innervation and were difficult to trace further. We classified the amygdaloid nuclei into three groups: (1) the deep or basolateral group (2) the superficial or cortical-like group and (3) the

335 centromedial group (McDonald, 1998). There were other nuclei which did not easily
336 incorporate into any of these groups, which we describe separately.

337 **3.3.1 Deep or basolateral group**

338 According to the aforementioned classification, the basolateral group includes the lateral
339 amygdalar nucleus (LA), basolateral amygdalar nucleus (BLA), and basomedial amygdalar
340 nucleus (BMA). LA nuclei were moderately (3+) labelled throughout the rostro-caudal extent,
341 though the density in its apical portion was less compared to the basal area (Figure 3C-E). We
342 noticed that BLA nuclei were among the most heavily innervated nuclei (Figure 3A-F). Among
343 its different subdivisions, both the anterior (BLAa) and posterior (BLAp) nuclei were very
344 densely (6+) labelled. However, the fiber density within BLAa decreased slightly at its caudal
345 extent. The ventral part (BLAv) was densely (5+) innervated (Figure 3D-E). Similarly, we
346 observed variations in the innervation density among the different subdivisions of BMA nuclei.
347 Its anterior part (BMAa) was densely (5+) labelled (figure 3A-B). However, the innervation
348 density in the posterior part (BMAp) increased from moderate (3+) (Figure 3C) to dense (5+)
349 (Figure 3E) level and then decreased again towards its caudal extent (Figure 3F).

350 **3.3.2 Superficial or cortical-like group**

351 Superficial or cortical-like group of amygdalar nuclei is also known as corticomedial nuclei. It
352 consists of nucleus of lateral olfactory tract (NLOT), bed nucleus of accessory olfactory tract
353 (BA), anterior and posterior cortical amygdalar nucleus (CoAa and CoAp), and the piriform-
354 amygdaloid area (PAA). We noticed that NLOT exhibited change in both the innervation
355 pattern and density along the rostro-caudal axis. It was densely (5+) innervated at its rostral
356 pole without a laminar pattern (fig not shown). At its midway along the rostro-caudal axis, it
357 appeared distinct because of slightly less innervation (4+) compared to its surrounding area
358 (Figure 3A). We observed a tri-laminar pattern at its caudal extent with a less innervated
359 intervening layer (layer 2) compared to the rest of the layers (4+) (Figure 3B). Similarly, BA

was moderately (3+) labelled (Figure 3B). We also observed that the innervation density within CoAa decreased from moderately high density (4+) to milder (2+) level (Figure 3A-B), whereas the density within CoAp increased from moderate (3+) (Figure 3C) to dense (5+) (Figure 3F) labelling pattern along the rostro-caudal axis. Similarly, fiber density within the PAA also increased from moderate (3+) to dense (5+) pattern (Figure 3C-F) rostro-caudally.

3.3.3 Centromedial group

The centromedial group consists of medial (MeA) and central amygdalar (CeA) nuclei. CeA nuclei were moderately (3+) labelled throughout the anteroposterior extent (Figure 3B-D) except at its moderately high (4+) labelled rostral most end (Figure 3A). We observed that medial amygdalar nucleus (MEA) exhibited heterogenicity among its different subdivisions. Its anterodorsal part (MEAad) received very dense (6+) to dense (5+) projection fibers along its rostro-caudal extent (Figure 3A-C). The anteroventral (MEAav) (Figure 3C-D), posteroventral (MEApv) (Figure 3E) and posterodorsal (MEApd) (Figure 3D-E) part were moderately (3+) labelled throughout the rostro-caudal axis. However, the boundaries of these nuclei had higher density fibers compared to the core.

3.3.4 Other nuclei

The nuclei that did not fit in the above classification include the anterior amygdalar area (AAA) (Figure 3A), intercalated areas (IA) (Figure 3A-C), and posterior amygdaloid nucleus (PA) (Figure 3F), all of which were heavily innervated (*See table 2*).

3.4 INNERVATION PATTERN IN THE SEPTUM

The septum has three major parts and their subdivisions. The major areas are the medial septum (MS), lateral septum (LS), and the nuclei of diagonal band (NDB) (Risold, 2004). We observed that highly fluorescent and thick collaterals of pathway fibers entered into the septum via NDB (Figure 4A), substantia innominata (SI) (Figure 5A) and via lateral preoptic area (LPO) (Figure 4E), which made the septum appear very rich in innervation. The septum served as the route

385 for these fibers to reach above the corpus callosum (CC) (where they clustered to form the
386 supracallosal bundle) (Figure 4A, arrow head) and into dorsal fornix (df) and fimbria (fi)
387 (Figure 7A & E, arrow). Finally, all these fibers culminated into the hippocampus (Figure 7E).
388 On a close inspection of the septal component, we noticed that few thin and varicosed fibers of
389 innervation were scattered among the thick collaterals of pathway fibers. Moreover, we
390 observed heterogenicity in the innervation density and orientation of fibers among the different
391 nuclei.

392 **3.4.1 The nucleus of diagonal band (NBD) and medial septum (MS)**

393 The NDB consists of two limbs, the vertical and horizontal limb (Figure 4C, D). The vertical
394 limb is in continuation with the medial septum (MS) and occupies the medial most position in
395 the rostral half of the septum (Figure 4B-D). Towards the rostral pole, we observed that the
396 medially diverted collaterals of ascending pathway fibers ran dorsally along the lateral border
397 of NDB and via the lateral septum (LSr) to reach above the CC, thus forming the supracallosal
398 bundle (SCB) (Figure 4A). The SCB ran caudally over the CC while providing the innervation
399 to the medial part of cortex en-route which finally turned around the splenium of CC to enter
400 into the hippocampus (Figure 7E). In the slight caudal section, some of the medially diverted
401 collaterals of ascending fiber ran dorsally along lateral border of NDB to continue into the MS
402 which then terminated upon surrounding the septo-hippocampal (SH) nuclei (Figure 4B). We
403 observed that at the midway septal level, majority of the fibers entering into the septum along
404 the lateral border of NDB appeared relatively straight and oriented ventro-dorsally to reach up
405 to the ventral border of CC (Figure 4C-D). They gave off many projections to the lateral septum
406 en-route. A particularly striking feature of NDB and MS of the mid-level septum was the
407 moderately (3+) innervated zone lying close to the midline (Figure 4C-D). This zone consisted
408 of mainly the thin fibers of innervation with very few collaterals of ascending pathway fibers.
409 The overall density and pattern of SERT-EGFP fibers in the MS were similar to that of NDB.

In addition, we observed a strikingly very dense (6+) cluster of fibers in the limiting zone between nucleus accumbens (NAc) and lateral septum (LSr) (Figure 4D, yellow arrow head).

3.4.2 Lateral septal nucleus

The lateral septum (LS) consists of three main subdivisions; the caudal (LSc), rostral (LSr) and ventral (LSv). We noticed heterogeneous distribution of SERT-EGFP fibers among the different subdivisions of the LS. The LSc was the least innervated area of the whole septum. It contained vertically oriented fibers at its border abutting the CC (Figure 4C-F, arrow head). Upon tracing these vertical fibers, we noticed they passed caudally into the dorsal fornix which served as one of the sources of innervation of the hippocampus (Figure 7A). The rest of the area of LSc had randomly oriented fibers in minimal density (1+) (Figure 4D-F). However, LSc was moderately labelled at its rostral pole (Figure 4C). Similarly, we found that LSv was moderately (3+) innervated (Figure 4E-F). However, the collaterals of ascending fiber entering into the septum were arborized heavily on its dorsomedial part (arrow head, Figure 4E). We observed that the LSr was among the densely labelled areas of the whole brain, however, it demonstrated heterogenicity in the labelling density and orientation of fibers along the rostro-caudal axis. It was very densely (6+) innervated in the rostral half (Figure 4A-B), densely (5+) with randomly oriented fibers at the mid-level (Figure 4C-D) and the density decreased even further towards its caudal pole (4+) where the fibers were mediolaterally oriented (Figure 4E). Upon tracing the fibers, we noticed that the collaterals of pathway fibers within the LSr passed caudally into septofimbrial nuclei (SF) (Figure 4F) and finally were projected into the fimbria. The fimbria (fi) served as one of the sources of innervation of hippocampus (Figure 7A & E). Thus, the medially diverted fibers from the main ascending bundle traversed across the different level of septum to reach the supracallosal bundle, fimbria and dorsal fornix which finally culminated into the hippocampus (Figure 7E).

3.4.3 Other Septal areas

435 There are other areas which are located within the septum but are not its principal components.
436 We observed that septo-hippocampal (SH) nucleus was sparsely (1+) innervated (Figure 4A-
437 B). However, the collaterals of pathway fibers running dorsally across MS terminated along its
438 outskirts (Figure 4B). Innervation in the insula magna (islm), the largest islands of Calleja,
439 exhibited the rostro-caudal gradient. The rostral *islm* that was almost devoid of the innervation
440 (Figure 4C) received dense (5+) network of fibers at its caudal extent (Figure 4D). Similarly,
441 column of fornix (fx) appeared completely devoid of the innervation except a thin fascicle of
442 fibers that was observed running dorsally in-between two bilateral columns which reached up
443 to the ventral border of CC (Figure 4E). Triangular septal nucleus (TRS) was sparsely (1+)
444 innervated (Figure 4F). However, SF contained mediolaterally oriented collaterals of pathway
445 fibers in moderately high (4+) density (Figure 4F).

446 **3.5 INNERVATION PATTERN IN THE BASAL GANGLIA**

447 We observed gradual increase in the labelling density of caudo-putamen (CP) rostro-caudally.
448 The mildly (2+) labelled CP towards its rostral extent (Figure 5A) received moderately high
449 (4+) projections towards its caudal pole (Figure 5E). We noticed that the collaterals of main
450 ascending bundle clustered in SI were diverted either medially or laterally to provide the
451 innervation to the CP (Figure 5A-D). The laterally directed fibers passed along external capsule
452 (ec) (Figure 5A, arrow head) and/or turned around the anterior commissure (aco) to innervate
453 the lateral part of CP (Figure 5B), whereas the medially directed collaterals of pathway fibers
454 passed dorsally across BNST around the *aco* to reach the medial side of CP (Figure 5C,
455 segmented black arrow line). Thus, because of these different routes of innervation, the density
456 of labelling in the CP was higher either laterally (Figure 5B) or medially (Figure 5C) at different
457 levels along the rostro-caudal extent. In addition, the collaterals of pathway fibers running
458 rostrally through CP were clustered together at some points which appeared as patches in the
459 coronal section (arrow Figure 5C, red arrow head). We noticed that the areas through which

thalamocortical fibers were traversing ahead appeared as circular gaps in the coronal sections as they were unlabeled with GFP (Figure 5C, green arrow head). The SERT-EGFP fibers surrounding these gaps gave it a whorl like appearance. In sagittal sections, the collaterals of pathway fibers entering into the CP via external capsule or GP can be distinguished as smooth, straight, large diameter structures which were more evident in the NAc (Figure 5F & G, red arrow head). The terminal fibers innervating CP were very fine in morphology. The GP received very dense (6+) serotonergic projection which made it clearly distinguishable from the adjacently located striatum (Figure 5D-E). The collaterals of main ascending fibers streamed into GP from lateral hypothalamic area (LHA) through SI (Figure 5E). In addition, we observed that the pattern of SERT-EGFP fibers in GP external segment (GPe) changed from a whorl pattern (Figure 5D) to homogeneous labelling (Figure 5E) rostro-caudally.

3.6 INNERVATION PATTERN IN THE NUCLEUS ACCUMBENS

The innervation pattern in the nucleus accumbens (NAc) was unique because of the presence of two different types of terminal fibers. We observed a unique type of fine, non-varicose, relatively straight terminals scattered among the ubiquitous punctate type of fibers of innervation. These unique types of terminal fiber had morphology similar to pathway fibers but were thin in diameter. They appeared as loosely clustered patch in the coronal sections of caudal NAc (Figure 5C, blue arrow head) and can be visualized much better in the sagittal sections (Figure 5F & G, red arrow head). We noticed that the innervation density in the NAc was higher rostrally (4+) (Figure 5A) than its caudal pole (3+) (Figure 5C). This was because the loosely clustered fibers at the caudal NAc were scattered throughout the nuclei at the rostral pole.

3.7 INNERVATION PATTERN IN THE BED NUCLEUS OF STRIA TERMINALIS

We observed that collaterals of pathway fibers clustered within substantia innominata (SI) were diverted medially which turned around the anterior commissure (aco) to reach the medial side

485 of CP; thus, innervating the bed nuclei of stria terminalis (BNST) en-route (Figure 6A-B and
486 5C). However, towards the caudal pole of BNST, the detached fibers from the main ascending
487 bundle at lateral preoptic area (LPO) entered into the BNST which then continued into the stria
488 terminalis (st) (Figure 6C-D). Those fibers in ST ran caudally above the thalamus to project
489 into the amygdala ultimately (Figure 3C-D). In the anterior division of BNST, we observed
490 that the SERT-EGFP fibers were distributed homogeneously in moderately high density (4+)
491 to dense (5+) levels within the anteromedial (am) and anterolateral (al) nuclei. However, the
492 density was mild (2+) in the oval (ov) and fusiform nuclei (fu) (Figure 6A-B). At the posterior
493 division of BNST, we noticed that anteromedial (am), anterolateral (al) and transverse nuclei
494 were very densely (6+) labelled. The rest of the nuclei had dense (5+) labeling except the
495 principal nuclei (pr) which was mildly (2+) labelled except on its ventral part (Figure 6C, D).

496 **3.8 INNERVATION PATTERN IN THE HIPPOCAMPUS**

497 Hippocampus constitutes of 4 major parts, viz: hippocampal formation (HPF), dentate gyrus
498 (DG), subiculum (SUB) and entorhinal area (ENT). HPF which is also known as cornu
499 ammonis (CA) is further subdivided into various zones, viz; CA1, CA2 and CA3. HPF consists
500 of four different layers; from outward to inward; viz: stratum oriens (SO), pyramidal layer (Py),
501 stratum radiatum (SR), stratum lacunosum moleculare (SLM), whereas, the DG comprises of
502 three layers viz; molecular layer (Mo), granule cell layer (SG) and polymorph layer (Po)
503 (Witter and Amaral, 2004).

504 We observed heterogeneously distributed SERT-EGFP fibers among the various layers
505 of hippocampus that gave it a laminar appearance. The SG of dentate gyrus was almost devoid
506 of the innervation, whereas fibers were sparsely (1+) scattered within SP and PO layers (Figure
507 7A-C). SLM was densely (5+) labelled in dorsal hippocampus (Figure 7B-C) which became
508 even more dense (6+) in the ventral hippocampus (Figure 7D). The compactly arranged fibers
509 within CA1 SLM were diffused laterally to distribute over the CA3 SR in moderately high (4+)

density (Figure 7B-C). Similarly, the fibers entering into the hippocampus via fimbria (fi) also labelled the CA3 SO in moderately high (4+) density. Therefore, except the CA3 SR and CA3 SO, the rest of the areas of these layers and the dorsal part of MO layer were moderately (3+) labelled, whereas the SERT-EGFP fibers were mildly scattered in the ventral part of MO layer (Figure 7B-C). The pattern in the ventral hippocampus was almost congruent with dorsal hippocampus (Figure 7D) except the labelling in SLM was higher than its dorsal counterpart.

We traced the fibers of innervation to the hippocampus which were derived through three different sources, viz; dorsal fornix (df), supracallosal bundle (scb) and fimbria (fi). The medially diverted collaterals from the main ascending bundle that traversed through septal nuclei were finally streamed into the scb, df and fi (Figure 7E) (also see the innervation to the septum above). The dorsal fornix was mainly responsible for the innervation of rostral pole of dorsal hippocampus (Figure 7A). The fibers from the fimbria projected into the hippocampus through laterally located CA3 zone (Figure 7A-C). The supracallosal fiber bundle ran caudally above the CC and turned around its splenium to terminate finally into the hippocampus (Figure 7C black arrow & E yellow arrow head). These fibers mainly streamed into the SLM and alveus and were subsequently distributed into the adjacent layers (Figure 7C). We noticed that the collaterals of pathway fibers within the SLM of ventral hippocampus passed externally to get heavily distributed over the rhinal areas (Figure 7D).

3.9 INNERVATION PATTERN IN THE CORTEX

We traced various routes of innervation of the cerebral cortex which varied depending on the brain levels. At the frontal pole of the brain, the collaterals of pathway fibers clustered within the substantia innominata (SI) passed laterally around the rhinal fissure (RF) to project mainly into cortical layer 1 (Figure 8B-C). Similarly, the fibers clustered within the endopiriform nuclei (EP) also streamed into the layer 1, 5 and 6b of lateral cortex (Figure 8C-D). The collateral pathway fibers running in the external capsule (ec) supplemented the innervation of

layer 6b and additionally innervated the lateral part of CP (Figure 8C-D, 5B-C arrow). The fibers were very densely (6+) distributed within the claustrum (CLA) (Figure 8C-D). We observed that the medial cortex had separate sources of innervation. It was innervated mainly by the collaterals of pathway fibers streaming through supracallosal bundle (scb) (Figure 7E, 8D & E), indusium griseum (ig) (Figure 8C & H, arrow), and medial cortical bundle (Figure 8C). We noticed that the outermost cortical layer was the most labelled (5+) layer having transversely oriented fibers to the horizontal axis. We observed difference in the innervation pattern among the various cortical areas and gradual decrease in the labelling density as traced rostro-caudally.

3.9.1 Prefrontal Cortex

The prefrontal cortex (PFC) of the mouse consists of three major parts, the medial (mPFC), orbital (ORB) and agranular insular cortices (AI). mPFC is further subdivided into prelimbic (PL), infralimbic (IL) and anterior cingulate area (ACA) (Allen Institute for Brain Science, 2004). We observed that these different areas exhibited heterogeneous innervation density and pattern along the rostro-caudal axis. At the rostral pole, the PL area had patch like fibers clustered within the upper layers in moderately high (4+) density (Figure 8A). However, the caudal extent of PL area (Figure 8C) and the whole rostro-caudal extent of ILA and ACA (Figure 8A-D) were moderately (3+) labelled except at layer 1 (Figure 8B-D). The fibers that entered into the mPFC via EP nuclei (Figure 8B) and medial cortical bundle (Figure 8C) ran vertically through its deeper layers. Similarly, the orbitofrontal cortex (ORB) exhibited an alternating laminar pattern towards its rostral extent (Figure 8A) which was less evident caudally especially on its medial (m) part (Figure 8B). Innervation of AI also appeared in a laminar pattern because of the readily identifiable layer 1 and 5 which received higher innervation compared to the intervening layer (Figure 8A-C). Traced more caudally, the

559 deepest layer (layer 6b) in AI cortex was also densely (5+) labelled because of fibers entering
560 into the lateral cortex through layer 1, 5 and 6b (Figure 8D).

561 **3.9.2 Retrosplenial cortex**

562 The retrosplenial cortex (RSP) contained a distinct vertical band of fibers running in parallel
563 to layer 1 at its rostral pole (Figure 8E & F). The fibers were moderately (3+) distributed (Figure
564 8E) which progressively decreased in density caudally (Figure 8F-G). The fibers clustered
565 within the supracallosal bundle (scb) was the source of innervation to the RSP cortex (Figure
566 8E, arrow).

567 **3.9.3 Motor cortex**

568 Motor cortex also exhibited the laminar innervation pattern. Similar to the other cortical areas,
569 layer 1 was distinct because of its dense (5+) innervation. Towards the rostral pole, layer 5 of
570 the primary motor cortex (MOp) was densely (5+) labelled (Figure 8A), which gradually
571 decreased in density (4+) as traced caudally (Figure 8B-E). The rest of the layers were
572 moderately (3+) labelled, thus giving it a laminar appearance. The fibers in layer 2/3 were
573 oriented vertically to the horizontal axis, whereas randomly distributed elsewhere (Figure 8D-
574 E). The MOp and secondary motor (MOs) area exhibited slight differences in the innervation
575 density only at its rostral pole (Figure 8A), whereas the patterns were almost similar elsewhere
576 (Figure 8B-E).

577 **3.9.4 Somatosensory cortex**

578 Rostral half of somatosensory (SS) cortex appeared distinct from the adjacent motor (MO)
579 cortex because of its densely (5+) labelled layer 5 and mildly (2+) labelled layer 2/3 and 4
580 (Figure 8B-D). However, the innervation density of layer 5 gradually decreased to moderately
581 high (4+) level towards its caudal extent (Figure 8E). Thus, SS cortex appeared similar to the
582 adjacent MO cortex at the caudal level (Figure 8E). We observed that the collaterals of pathway
583 fibers passing within the external capsule (ec) and claustrum (CLA) densely (5+) arborized in

584 the barrel field (bf) area (Figure 8D). The higher labelling of layer 1, 5 and 6b compared to the
585 intervening layers made the innervation pattern alternatingly laminar in SS cortex (Figure 8B-
586 E). Basically, we found no difference in innervation pattern between the primary and secondary
587 SS cortex. The overall innervation density in the SS cortex decreased rostro-caudally.

588 **3.9.5 Auditory and visual cortexes**

589 The auditory and visual cortices which are located towards the caudal pole of the mouse brain
590 received relatively less serotonergic innervation compared to the rostrally located cortical
591 regions like the motor and somatosensory cortices (Figure 8F-G & 7D). The outer most layer
592 1 was thin but densely (5+) innervated. The underlying layer 2/3 and 4 were sparsely (1+)
593 innervated (Figure 8F-G & 7D), however, the innervation density in rest of the layers decreased
594 from moderate (3+) labeling in the rostral half (Figure 8F-G) to milder (2+) density towards
595 the caudal end (Figure 7D). Thus, the overall innervation density in the auditory and visual
596 cortex also progressively decreased rostro-caudally (Figure 8F-G & 7D).

597 **3.9.6 Rhinal Area**

598 The rhinal cortex was the most labelled cortical area. At its rostral extent, all the layers except
599 the layer 2/3 were densely (5+) innervated (Figure 8F). However, towards its caudal pole, layer
600 2/3 and the deepest layer were mildly (2+) innervated while the others received very dense (6+)
601 innervation (Figure 7D). We observed that the collaterals of pathway fibers running across the
602 stratum lacunosum moleculare (slm) of the ventral hippocampus moved outside of it to
603 heavily innervate the laterally located rhinal cortex (Figure 7D).

604 **3.9.7 Piriform cortex**

605 In this three-layered structure, the rostral extent of piriform cortex (PIR) was moderately (3+)
606 labelled without laminar appearance (Figure 8D). However, a laminar pattern was observed in
607 the caudal PIR where the outer layer was densely (5+) labelled and appeared distinct from
608 underlying layer 2 and 3 which were moderately (3+) labelled (Figure 3C).

609 **3.10 INNERVATION PATTERN IN THE OLFACTORY TUBERCLE and**
610 **OLFACTORY BULB**

611 We observed densely (5+) distributed thick and tortuous fibers clustered around the island of
612 Calleja (isl) within the rostral extent of olfactory tubercle (OT) (Figure 6A-B), while the *isl*
613 being almost devoid of the innervation. However, the caudal OT was innervated with
614 homogenously distributed fine fibers in slightly less density compared to its rostral counterparts
615 (Figure 6C-D). The OT and SI served as the route for the ascending forebrain bundle to traverse
616 rostrally towards the olfactory bulb (Figure 6A).

617 Main olfactory bulb (MOB) was the terminal projection site of the ascending forebrain
618 bundle arising from the midbrain raphe nuclei (Figure 9A). Fibers in MOB were arranged in a
619 laminar pattern. We noticed that the outer most glomerular (GL) layer was densely (5+)
620 innervated with SERT-EGFP fibers. Mitral (MI), internal plexiform (iPL) and granule (GR)
621 cell layers were readily undistinguishable because of the homogeneously distributed fibers in
622 moderately high (4+) density. The outer plexiform layer (OPL) and olfactory ventricles (OV)
623 were sparsely (1+) labelled. We noticed that glomerular fibers were thick in diameter, intensely
624 labelled and contained large varicosities, while thinner fibers predominated in the
625 infraglomerular layers. The olfactory nerve layer (onl) was completely devoid of the
626 serotonergic projections (Figure 9A-B).

627 The accessory olfactory bulb (AOB) was devoid of the innervation, except the few
628 sparsely (1+) scattered fibers within the granular (gr) layer (Figure 9B).

629 **3.11 INNERVATION PATTERN IN THE CEREBELLUM**

630 Cerebellum was the least innervated major brain component (Figure 10). Few fibers (1+) were
631 distributed within the Purkinje cell layer (pr) and granular layer (gr). Molecular layer (mo) and
632 white matter (wm) appeared unlabeled. Surprisingly, we observed that deep cerebellar nuclei
633 were moderately (3+) labelled because of the direct projection from the raphe nuclei.

634 *The results for each brain region and their nuclei are tabulated in the table 2.*

635 **4. DISCUSSION**

636 The serotonergic system is one of the diffusively organized brain neuronal systems. Although
637 the cellular localization and projections map was first described long ago with the advent of
638 histofluorescence technique (Dahlström and Fuxe, 1964), the improved topographical
639 description was possible only after the development of antibodies against the enzyme
640 tryptophan hydroxylase (Pickel et al., 1977) or the putative neurotransmitter 5-HT itself
641 (Steinbusch, 1981). However, these techniques were accompanied with certain limitations. In
642 order to overcome the limitations of earlier studies, we employed the genetically engineered
643 transgenic mice expressing GFP in the 5-HT transporter. Using this mouse model, we
644 attempted to provide more comprehensive map of the terminal field of serotonergic neurons
645 than is currently available. In the following section, we highlight some of our results, compare
646 them with those of previous studies and discuss the possible functional implications.

647 The serotonergic neurons projecting to the forebrain originated from the rostral group
648 of raphe nuclei in the midbrain and virtually innervated all the brain regions with striking
649 density in the hypothalamus, septal nuclei, thalamus, amygdala, olfactory bulb followed by
650 basal nuclei and cortex. Except the white matter structures, there was hardly no brain region
651 that did not receive 5-HT innervation. This was consistent with the previous findings
652 (Steinbusch, 1981). We observed two different types of innervation fibers; fibers with large
653 and spherical varicosities and fine fibers with small and granule shaped varicosities. Previous
654 studies have shown that the difference in fiber morphology possesses functional significance.
655 For instance, the fine 5-HT axon terminals are supposed to be extremely vulnerable to
656 psychotropic drugs like amphetamine (O'Hearn et al., 1988). Similarly, change in the ratio of
657 these fiber types has been observed in epilepsy where fibers with small-sized varicosities were
658 decreased in the dentate gyrus of hippocampus, infralimbic cortex and medial septum while

659 that of the fibers with larger-sized varicosities were increased (Maia et al., 2019). Moreover,
660 changes in the morphology of serotonergic fibers associated with aging have been reported
661 (Nishimura et al., 1998). Thus, analysis of 5-HT structural system could help understand the
662 pathophysiology of mental disorders and lead to drug discovery. The 5-HT projection
663 demonstrated an extensive and very specific innervation pattern in the brain areas as discussed
664 below.

665 **4.1 Thalamus**

666 SERT-EGFP fibers were mainly concentrated in midline thalamus (paraventricular, paratenial,
667 rhomboid and reuniens nuclei), rostral part of intralaminar thalamus (central medial and central
668 lateral nuclei), some part of anterior thalamus (anteroventral, rostral part of intermediodorsal
669 nuclei) and in the other nuclei like lateral dorsal nucleus (LD), lateral posterior nucleus (LP)
670 and lateral geniculate (LG) complex etc.

671 Most of the previous findings of thalamic mapping using peroxidase-antiperoxidase
672 (PAP) technique were consistent to ours (Cropper et al., 1984). However, they reported light
673 labeling in several nuclei like mediodorsal, centromedian, and subthalamic nuclei where we
674 found fibers in comparatively higher densities. Conversely, we found very light labelling in
675 caudal part of reticular nuclei, ventral medial nuclei and posterior nuclei which they reported
676 to be moderately labelled. Similar to us, other studies have also reported that principal thalamic
677 nuclei lack the serotonergic input (Vertes et al., 1999). We observed very distinct distribution
678 of fibers across the rostro-caudal axis of the reticular nuclei that progressively decreased in
679 their density towards their caudal pole. This contrasts with the findings of one of the
680 immunohistochemical studies which reported to have little difference (Rodríguez et al., 2011).
681 We noticed some species differences as well. Similar to mice, the non-specific nuclei in primate
682 (squirrel monkey) received the heaviest innervation. However, the lightly labelled reticular

683 nuclei in mice were heavily labelled in the monkey, whereas, the richly innervated nuclei in
684 mice such as AV, LD, and LGd were less innervated in the monkey (Lavoie and Parent, 1991).
685 Studies have shown that the midline thalamic nuclei in connection with limbic
686 subcortical and cortical sites (Su and Bentivoglio, 1990) exert an arousing effect on the limbic
687 forebrain (Vertes, 2006). The high density of 5-HT innervation in these nuclei suggests that
688 they might modulate the emotional and cognitive functions. Similarly, the proposal of anterior
689 thalamic nuclei as an extended component hippocampal-dependent memory network,
690 (Aggleton and Brown, 1999) suggests that high serotonergic innervation in these nuclei might
691 exert some effect on episodic memory. Projections of large numbers of SERT-EGFP fibers to
692 the lateral dorsal nuclei (LD) and lateral geniculate nuclei suggest that it might modulate
693 visually guided spatial navigation and learning (Mizumori et al., 1994) or may sharpen the
694 visuospatial processing activity (Groenewegen and Witter, 2004). Similarly, studies have
695 reported that the downregulation of serotonergic system in the lateral habenula is linked with
696 the depressive symptoms in patients with Parkinson's disease (Sourani et al., 2012). However,
697 the precise role served by 5-HT in various thalamic nuclei and their function remains to be
698 fully determined.

699 **4.2 Hypothalamus**

700 We observed that the hypothalamic nuclei received strong SERT-EGFP fiber input with
701 exceptions in some nuclei. The ascending forebrain bundle traversed rostrally through the
702 lateral hypothalamic area (LHA) and lateral preoptic (LPO) nuclei which made them appear
703 over crowded. There are some older reports showing 5-HT projections in hypothalamus.
704 However, some of them had employed older autoradiographic technique and did not cover all
705 the nuclei (Beaudet and Descarries, 1979), while another had used antibody against 5-HT but
706 without the monoamine oxidase inhibitor treatment (Steinbusch, 1981). Although the patterns
707 reported in many of the nuclei were similar to us, we observed higher labelling density in many

of the nuclei than their reports because of the superiority of the technique used. None of these previous studies have reported the changes in the labelling pattern in the different hypothalamic nuclei across the rostro-caudal axis.

Some earlier studies have reported the presence of serotonergic cell bodies in the dorsomedial hypothalamic nucleus of rats (Fuxe et al., 1968) (Beaudet and Descarries, 1979) but we did not detect any such cell bodies in hypothalamus. We think that this might be a technical limitation in autoradiographic technique where some non-specific neurons might have absorbed infused 5-HT. A study employing antibody against 5-HT in guinea pig brain also did not detect such cell bodies in hypothalamus (Warembourg and Poulain, 1985).

The ventromedial part of the SCN was one of the highest labelled nuclei in the whole brain. The finding corroborates with results from other rodent models such as hamster (Legutko and Gannon, 2001) and rat (Steinbusch, 1981), and is also consistent with humans (Borgers et al., 2014). According to the earlier tracing studies, SCN receives very dense projections from the median raphe (MR), but not from the DR (Meyer-Bernstein and Morin, 1996) (Muzerelle et al., 2016). Therefore, it can be hypothesized that depletion of 5-HT in the MR or the destruction of 5-HT fibers restricted to the SCN could affect the circadian rhythm. Some previous reports have shown that 5-HT activity on the SCN inhibits the effects of light on the circadian system (Meyer-Bernstein and Morin, 1996) (Bradbury et al., 1997). Moreover, it is reported that the release of 5-HT at the SCN follows the daily rhythm and the behavioral state can strongly influence the serotonergic activity in the circadian clock (Dudley et al., 1998). This strong innervation of 5-HT fibers to the SCN suggests the reciprocal connections of the 5-HT and circadian systems and they may have importance for neurodevelopmental and psychiatric disorders such as ASD and mood disorders, respectively (Ciarleglio et al., 2011) (Takumi et al., 2019).

732 We noticed an interesting innervation pattern in hypothalamic nuclei regulating the
733 hunger and food intake. The arcuate nucleus was one of the least innervated hypothalamic
734 nuclei. The dorsomedial nucleus exhibited a rostro-caudal innervation gradient. The
735 ventromedial hypothalamic and paraventricular nuclei exhibited both rostro-caudal and
736 intranuclear innervation gradients. The lateral hypothalamic area was too crowded because of
737 the ascending forebrain bundle traversing through it. However, how these wide variations in 5-
738 HT-innervation of these nuclei affect the hunger mechanism is yet to be fully understood. Some
739 studies in mice have shown that there is inverse relationship between brain 5-HT and food
740 intake (Lam et al., 2010).

741 **4.3 Amygdala**

742 We observed that most of the amygdalar nuclei received SERT-EGFP fibers in high density
743 except the few nuclei such as lateral amygdala (LA), central amygdala (CeA) and medial
744 amygdala (MeA) were comparatively less innervated. Some of the previous studies have
745 reported serotonergic innervation patterns in the amygdaloid complex using various techniques
746 such as autoradiography (Parent et al., 1981), antibodies against 5-HT (Steinbusch, 1981) or 5-
747 HT transporter (Sur et al., 1996), in situ hybridization (Bonn et al., 2013) and electron
748 microscopy (Muller et al., 2007). However, most of them had either studied only the selected
749 amygdaloid nuclei or have reported lighter density compared to us which might be due to the
750 technical limitations. However, the common finding was that 5-HT fibers distribute densely to
751 the BLA and BMA but less heavily to the LA and CeA nuclei. This was also consistent with
752 the findings reported in a recent review (Asan et al., 2013). In addition, a recent study also
753 showed that BLA is the most labelled nuclei among the different limbic structures which are
754 in the sequence of BLA > NAc > BNST >HIP > CeA > mPFC (Belmer et al., 2017). An
755 anterograde tracing study has reported that amygdalar nuclei receive serotonergic efferents
756 mainly from the DR and very minor projections from the MR (Muzerelle et al., 2016).

We noticed striking species differences in the distribution patterns of SERT-EGFP fibers. On contrary to the rodent pattern, the fiber densities in non-human primate were in the order of central nucleus > basolateral complex > medial nucleus (O'Rourke and Fudge, 2006) (Zeng et al., 2006), while in the human amygdala sequence followed: cortical and anterior amygdaloid nuclei > basolateral and central nuclei (Storvik et al., 2007). Differential expression of the SERT has been linked to species variation in sensitivity to social cues, vigilance to social threats, risk avoidance, responsiveness to changes in reward contexts and mood (Vallender et al., 2009).

Functionally, the BLA is positioned at the pivotal point in the amygdalar circuitry to modify the information received from LA to CeA nuclei (Amano et al., 2011). Coupling this fact with the presence of very dense 5-HT innervation suggests that it could be the primary amygdalar target for 5-HT neuromodulation of fear and anxiety. This is supplemented by findings from a recent pharmacological study which showed that depletion of 5-HT in the BLA reduces anxiety and fear (Johnson et al., 2015). Similarly, action of oxytocin on the MeA nuclei in facilitating the social recognition (Ferguson et al., 2001) could be coupled with the presence of heavy 5-HT innervation in MEAad as the common target for both in modulating the social recognition. Additionally, the decrease in density of 5-HT axons in the CeA and BLA and in the CA3 of the hippocampus due to postnatal social isolation has been linked to depression (Kuramochi and Nakamura, 2009).

4.4 Basal Ganglia

We observed fibers in higher density in globus pallidus (GP) compared to caudo-putamen (CP) which contrast with the findings of earlier immunohistochemical studies where no difference in the distribution density was reported (Steinbusch, 1981). Within the CP, fiber densities were higher either ventrolaterally or ventromedially depending on the brain levels which was congruent with a similar study (Mori et al., 1985). Similar to an earlier study (Ternaux et al.,

782 1977) we observed that the innervation density in the striatum increases rostro-caudally. The
783 distribution density of SERT-EGFP fibers demonstrated in our study was consistent with the
784 amount of 5-HT detected in different parts of striatum by liquid chromatography (Beal and
785 Martin, 1985). Similarly, we noticed higher SERT-EGFP fiber density in the external segment
786 (GPe) than the internal segment (GPi) of GP. This pattern was consistent even in primates (Eid
787 et al., 2013). Studies have reported that the innervation pattern in striatum is shared in both
788 rodent and non-human primates (Mori et al., 1985). A recent tracing study showed that striatum
789 and GP receive projection mainly from the supralemiscal (B9) group and minorly from the DR
790 and MR (Muzerelle et al., 2016).

791 The high serotonergic innervation in the GP suggests that it might be the pivotal site
792 for the 5-HT involvement in the basal ganglia functions or pathophysiology, although it is yet
793 to be confirmed. However, a study has shown that 5-HT influences the reward seeking circuitry
794 involving GPi and lateral habenula (Hong and Hikosaka, 2008). Similarly, the result from one
795 of the studies showing the preferential loss of striatal SERT fibers in Parkinson disease (PD)
796 (Kish et al., 2007) indicates the involvement of 5-HT along with dopamine in the PD
797 pathophysiology. A recent study showed that 5-HT affects the synaptic signaling at
798 thalamostriatal inputs (Cavaccini et al., 2018) which suggests that striatal-dependent functions
799 may be subjected to serotonergic modulation.

800 **4.5 Cortex**

801 We found densely concentrated SERT-EGFP fibers in the alternating layers of cortical areas
802 such as mPFC, insular cortex, somatosensory cortex, piriform and rhinal cortices. This was in
803 contrary to the previous immunohistochemical report where they mentioned the uniform
804 distribution of fibers across all the cortical layers (Lidov et al., 1980). Similar to us, one of the
805 immunohistochemical studies reported that the elaborated radial plexus innervates the upper
806 layers and the tangential fibers course through the deeper layers of prelimbic cortex (Miner et

al., 2000). We noticed that prelimbic cortex that projects to the limbic areas received higher projection fibers compared to non-limbic regions (i.e. ACC). This could possibly explain the underlying role of 5-HT on the emotional, behavioral and cognitive functions. Any alteration could possibly subserve the pathophysiology of many mental disorders. For instance, reductions in the length of SERT fibers in the orbitofrontal cortex have been found in the postmortem brain of the patient with major depressive disorder (Rajkowska et al., 2017). Similarly, reduced SERT-ir fiber density in the medial frontal cortex, midbrain, and temporal lobe areas have been reported in the autistic brain (Makkonen et al., 2008). A study that employed radiographic techniques reported the prelimbic and rostral agranular insula as the most densely labeled cortical areas sites (Audet et al., 1989). However, in our case we noticed that some other areas like somatosensory (layer 5) and rhinal cortices were equally or even more densely innervated compared to PLA and AI. Anterograde tracing study has shown that both DR and MR projects to prefrontal cortex with DR being the primary source (Muzerelle et al., 2016).

Next, we noticed species difference in the cortical layer labelling density. In our rodent model, a lightly labelled layer 2/3 intervene between moderately labelled superficial and deeper layers of the visual cortex. In the adult cat visual cortex, dense fibers were distributed within the layers I and III (Gu et al., 1990). In monkey, layer IV was the highest labelled layer visual cortical layer, whereas other layers received either less dense or very sparse labelling (Morrison et al., 1982).

Similarly, we observed dense projection within the barrel field area of the somatosensory cortex suggesting its significant role in modulating sensory information. Developmental studies have already demonstrated that 5-HT plays a significant role in the development of barrel formation in cortex (Persico et al., 2000). Not limited to the barrel field, compelling evidence suggests that 5-HT is necessary for the maturation, dendritic arborization,

832 migration, differentiation of many different kinds of neurons and interneurons which are
833 essential for the refined organization of the cerebral cortex (Vitalis et al., 2007).

834 **5. Conclusion**

835 In conclusion, we mapped the distribution pattern of the serotonergic neurons across the whole
836 brain region using SERT-EGFP model mice. The use of transgenic animal helped to elucidate
837 the topography of serotonergic system in much greater detail. We identified higher density of
838 projections than previously reported and observed that the densities and pattern changes along
839 the rostro-caudal brain axis. Although serotonergic fibers were ubiquitously distributed in the
840 brain, there was a defined topographic organization of these projections with strikingly high
841 projections in some specific targets. With a couple of exceptions, many of the nuclei with high
842 serotonergic projections were anatomically linked to forebrain limbic structures, suggesting
843 that 5-HT has modulatory effects on emotional and cognitive behaviors. A detailed analysis of
844 the topographical distribution of these neuronal populations will provide an anatomical basis
845 to postulate the physiological role of 5-HT in different behavior and in the understanding of
846 possible alteration in numerous mental and psychiatric disorders.

847

848 **Acknowledgement**

849 The authors express sincere thanks to Tsuyoshi Toya, Jun Nomura and Takeshi Kaizuka for
850 their useful help and discussions and all the technical staff of the Takumi Lab for their technical
851 assistance.

852 **Authors contribution**

853 All authors together conceived and designed the experiments. JRA drafted the manuscript,
854 collected the data and carried out the analysis with advice from KT and TT. All authors were
855 involved in the discussion and editing of the final manuscript. TT supervised the project.

856 **Competing Interests:** The authors declare that they have no competing interests.

857 **References**

858 Abe K, Shimada R, Okada Y, Kibayashi K. 2016. Traumatic brain injury decreases serotonin
859 transporter expression in the rat cerebrum. Neurol Res 38:358–363.
860 Aggleton JP, Brown MW. 1999. Episodic memory, amnesia, and the hippocampal-anterior
861 thalamic axis. Behav Brain Sci 22:425–44; discussion 444-89.
862 Allen Institute for Brain Science. 2004. Allen Mouse Brain Atlas. Available from:
863 http://atlas.brain-map.org/
864 Amano T, Duvarci S, Popa D, Pare D. 2011. The Fear Circuit Revisited: Contributions of the
865 Basal Amygdala Nuclei to Conditioned Fear. J Neurosci 31:15481–15489.
866 Asan E, Steinke M, Lesch KP. 2013. Serotonergic innervation of the amygdala: Targets,
867 receptors, and implications for stress and anxiety. Histochem Cell Biol 139:785–813.
868 Audet MA, Descarries L, Doucet G. 1989. Quantified regional and laminar distribution of the
869 serotonin innervation in the anterior half of adult rat cerebral cortex. J Chem Neuroanat
870 2:29–44.
871 Azmitia E, Gannon P. 1983. The ultrastructural localization of serotonin immunoreactivity in
872 myelinated and unmyelinated axons within the medial forebrain bundle of rat and monkey.
873 J Neurosci 3:2083–90.
874 Beal MF, Martin JB. 1985. Topographical dopamine and serotonin distribution and turnover in
875 rat striatum. Brain Res 358:10–15.
876 Beaudet A, Descarries L. 1979. Radioautographic characterization of a serotonin-accumulating
877 nerve cell group in adult rat hypothalamus. Brain Res 160:231–243.
878 Belmer A, Klenowski PM, Patkar OL, Bartlett SE. 2017. Mapping the connectivity of serotonin
879 transporter immunoreactive axons to excitatory and inhibitory neurochemical synapses in
880 the mouse limbic brain. Brain Struct Funct 222:1297–1314.
881 Berger M, Gray JA, Roth BL. 2009. The Expanded Biology of Serotonin. Annu Rev Med

882 60:355–366.
883 Bonn M, Schmitt A, Lesch K-P, Van Bockstaele EJ, Asan E. 2013. Serotonergic innervation
884 and serotonin receptor expression of NPY-producing neurons in the rat lateral and
885 basolateral amygdaloid nuclei. Brain Struct Funct 218:421–435.
886 Borgers AJ, Koopman KE, Bisschop PH, Serlie MJ, Swaab DF, Fliers E, la Fleur SE,
887 Alkemade A. 2014. Decreased serotonin transporter immunoreactivity in the human
888 hypothalamic infundibular nucleus of overweight subjects. Front Neurosci 8:106.
889 Bradbury MJ, Dement WC, Edgar DM. 1997. Serotonin-containing fibers in the
890 suprachiasmatic hypothalamus attenuate light-induced phase delays in mice. Brain Res
891 768:125–34.
892 Cavaccini A, Gritti M, Giorgi A, Locarno A, Heck N, Migliarini S, Bertero A, Mereu M,
893 Margiani G, Trusel M, Catelani T, Marotta R, De Luca MA, Caboche J, Gozzi A,
894 Pasqualetti M, Tonini R. 2018. Serotonergic Signaling Controls Input-Specific Synaptic
895 Plasticity at Striatal Circuits. Neuron 98:801-816.e7.
896 Ciarleglio CM, Resuehr HES, McMahon DG. 2011. Interactions of the serotonin and circadian
897 systems: Nature and nurture in rhythms and blues. Neuroscience 197:8–16.
898 Cropper EC, Eisenman JS, Azmitia EC. 1984. An immunocytochemical study of the
899 serotonergic innervation of the thalamus of the rat. J Comp Neurol 224:38–50.
900 D. G. Stuart. 1962. Anatomy of the Hypothalamus-and Its Connections (AAL-TDR-62-13 407
901 ’ 091). Los Angeles.
902 Dahlström A, Fuxe K. 1964. Localization of monoamines in the lower brain stem. Experientia
903 20:398–9.
904 Dudley TE, DiNardo LA, Glass JD. 1998. Endogenous regulation of serotonin release in the
905 hamster suprachiasmatic nucleus. J Neurosci 18:5045–52.
906 Eid L, Champigny M-F, Parent A, Parent M. 2013. Quantitative and ultrastructural study of

907 serotonin innervation of the globus pallidus in squirrel monkeys. Eur J Neurosci 37:1659–
908 1668.
909 Ferguson JN, Aldag JM, Insel TR, Young LJ. 2001. Oxytocin in the medial amygdala is
910 essential for social recognition in the mouse. J Neurosci 21:8278–85.
911 Fuxe K. 1965. Evidence for the existence of monoamine neurons in the central nervous system.
912 Iv. Distribution of monoamine nerve terminals in the central nervous system. Acta Physiol
913 Scand Suppl:SUPPL 247:37+.
914 Fuxe K, Hökfelt T, Ungerstedt U. 1968. Localization of indolealkylamines in CNS. Adv
915 Pharmacol 6:235–51.
916 Gong S, Zheng C, Doughty ML, Losos K, Didkovsky N, Schambra UB, Nowak NJ, Joyner A,
917 Leblanc G, Hatten ME, Heintz N. 2003. A gene expression atlas of the central nervous
918 system based on bacterial artificial chromosomes. Nature 425:917–925.
919 Groenewegen HJ, Witter MP. 2004. Thalamus. Rat Nerv Syst:407–453.
920 Gu Q, Patel B, Singer W. 1990. The laminar distribution and postnatal development of
921 serotonin-immunoreactive axons in the cat primary visual cortex. Exp brain Res 81:257–
922 66.
923 Harrington B. 2005. Draw Freely | Inkscape. Available from: https://inkscape.org/
924 Hong S, Hikosaka O. 2008. The Globus Pallidus Sends Reward-Related Signals to the Lateral
925 Habenula. Neuron 60:720–729.
926 Hrovatin K, Kunej T, Dolžan V. 2019. Genetic variability of serotonin pathway associated with
927 schizophrenia onset, progression, and treatment. Am J Med Genet Part B Neuropsychiatr
928 Genet.
929 Ishimura K, Takeuchi Y, Fujiwara K, Tominaga M, Yoshioka H, Sawada T. 1988. Quantitative
930 analysis of the distribution of serotonin-immunoreactive cell bodies in the mouse brain.
931 Neurosci Lett 91:265–70.

932 Johnson PL, Molosh A, Fitz SD, Arendt D, Deehan GA, Federici LM, Bernabe C, Engleman
933 EA, Rodd ZA, Lowry CA, Shekhar A. 2015. Pharmacological depletion of serotonin in
934 the basolateral amygdala complex reduces anxiety and disrupts fear conditioning.
935 Pharmacol Biochem Behav 138:174–179.
936 Kish SJ, Tong J, Hornykiewicz O, Rajput A, Chang L-J, Guttman M, Furukawa Y. 2007.
937 Preferential loss of serotonin markers in caudate versus putamen in Parkinson's disease.
938 Brain 131:120–31.
939 Kuramochi M, Nakamura S. 2009. Effects of postnatal isolation rearing and antidepressant
940 treatment on the density of serotonergic and noradrenergic axons and depressive behavior
941 in rats. Neuroscience 163:448–455.
942 Lam DD, Garfield AS, Marston OJ, Shaw J, Heisler LK. 2010. Brain serotonin system in the
943 coordination of food intake and body weight. Pharmacol Biochem Behav 97:84–91.
944 Lavoie B, Parent A. 1991. Serotoninergic innervation of the thalamus in the primate: An
945 immunohistochemical study. J Comp Neurol 312:1–18.
946 Legutko R, Gannon RL. 2001. Serotonin transporter localization in the hamster
947 suprachiasmatic nucleus. Brain Res 893:77–83.
948 Lidov HGW, Grzanna R, Molliver ME. 1980. The serotonin innervation of the cerebral cortex
949 in the rat-an immunohistochemical analysis. Neuroscience 5:207–227.
950 Lin SH, Lee LT, Yang YK. 2014. Serotonin and mental disorders: A concise review on
951 molecular neuroimaging evidence. Clin Psychopharmacol Neurosci 12:196–202.
952 Maciag D, Simpson KL, Coppinger D, Lu Y, Wang Y, Lin RCS, Paul IA. 2006. Neonatal
953 antidepressant exposure has lasting effects on behavior and serotonin circuitry.
954 Neuropsychopharmacology 31:47–57.
955 Maia GH, Soares JI, Almeida SG, Leite JM, Baptista HX, Lukoyanova AN, Brazete CS,
956 Lukoyanov N V. 2019. Altered serotonin innervation in the rat epileptic brain. Brain Res

957 Bull 152:95–106.
958 Makkonen I, Riikonen R, Kokki H, Airaksinen MM, Kuikka JT. 2008. Serotonin and dopamine
959 transporter binding in children with autism determined by SPECT. Dev Med Child Neurol
960 50:593–597.
961 McDonald AJ. 1998. Cortical pathways to the mammalian amygdala. Prog Neurobiol 55:257–
962 332.
963 Meyer-Bernstein EL, Morin LP. 1996. Differential serotonergic innervation of the
964 suprachiasmatic nucleus and the intergeniculate leaflet and its role in circadian rhythm
965 modulation. J Neurosci 16:2097–111.
966 Miner LH, Schroeter S, Blakely RD, Sesack SR. 2000. Ultrastructural localization of the
967 serotonin transporter in superficial and deep layers of the rat prelimbic prefrontal cortex
968 and its spatial relationship to dopamine terminals. J Comp Neurol 427:220–34.
969 Mizumori SJY, Miya DY, Ward KE. 1994. Reversible inactivation of the lateral dorsal
970 thalamus disrupts hippocampal place representation and impairs spatial learning. Brain
971 Res 644:168–174.
972 Mori S, Ueda S, Yamada H, Takino T, Sano Y. 1985. Immunohistochemical demonstration of
973 serotonin nerve fibers in the corpus striatum of the rat, cat and monkey. Anat Embryol
974 (Berl) 173:1–5.
975 Morrison JH, Foote SL, Molliver ME, Bloom FE, Lidov HG. 1982. Noradrenergic and
976 serotonergic fibers innervate complementary layers in monkey primary visual cortex: an
977 immunohistochemical study. Proc Natl Acad Sci 79:2401–2405.
978 Muller JF, Mascagni F, McDonald AJ. 2007. Serotonin-immunoreactive axon terminals
979 innervate pyramidal cells and interneurons in the rat basolateral amygdala. J Comp Neurol
980 505:314–335.
981 Muzerelle A, Scotto-Lomassese S, Bernard JF, Soiza-Reilly M, Gaspar P. 2016. Conditional

anterograde tracing reveals distinct targeting of individual serotonin cell groups (B5–B9) to the forebrain and brainstem. Brain Struct Funct 221:535–561.

Nielsen K, Brask D, Knudsen GM, Aznar S. 2006. Immunodetection of the serotonin transporter protein is a more valid marker for serotonergic fibers than serotonin. Synapse 59:270–276.

Nishimura A, Ueda S, Takeuchi Y, Matsushita H, Sawada T, Kawata M. 1998. Vulnerability to aging in the rat serotonergic system. Acta Neuropathol 96:581–595.

O'Hearn E, Battaglia G, De Souza EB, Kuhar MJ, Molliver ME. 1988. Methylenedioxyamphetamine (MDA) and methylenedioxymethamphetamine (MDMA) cause selective ablation of serotonergic axon terminals in forebrain: immunocytochemical evidence for neurotoxicity. J Neurosci 8:2788–803.

O'Rourke H, Fudge JL. 2006. Distribution of Serotonin Transporter Labeled Fibers in Amygdaloid Subregions: Implications for Mood Disorders. Biol Psychiatry 60:479–490.

Okaty BW, Commons KG, Dymecki SM. 2019. Embracing diversity in the 5-HT neuronal system. Nat Rev Neurosci 20:397–424.

Parent A, Descarries L, Beaudet A. 1981. Organization of ascending serotonin systems in the adult rat brain. A radioautographic study after intraventricular administration of [3h]5-hydroxytryptamine. Neuroscience 6:115–138.

Persico AM, Altamura C, Calia E, Puglisi-Allegra S, Ventura R, Lucchese F, Keller F. 2000. Serotonin Depletion and Barrel Cortex Development: Impact of Growth Impairment vs. Serotonin Effects on Thalamocortical Endings. Cereb Cortex 10:181–191.

Pickel VM, Joh TH, Reis DJ. 1977. A serotonergic innervation of noradrenergic neurons in nucleus locus coeruleus: demonstration by immunocytochemical localization of the transmitter specific enzymes tyrosine and tryptophan hydroxylase. Brain Res 131:197–214.

1007 Pollak Dorocic I, Fürth D, Xuan Y, Johansson Y, Pozzi L, Silberberg G, Carlén M, Meletis K.
1008 2014. A Whole-Brain Atlas of Inputs to Serotonergic Neurons of the Dorsal and Median
1009 Raphe Nuclei. Neuron 83:663–678.
1010 Rajkowska G, Mahajan G, Legutko B, Challagundla L, Griswold M, Albert PR, Daigle M,
1011 Miguel-Hidalgo JJ, Austin MC, Blakely RD, Steffens DC, Stockmeier CA. 2017. Length
1012 of axons expressing the serotonin transporter in orbitofrontal cortex is lower with age in
1013 depression. Neuroscience 359:30–39.
1014 Rasband W. 1997. ImageJ. U S Natl Institutes Heal Bethesda, Maryland, USA, [Internet].
1015 Available from: https://imagej.nih.gov/ij/
1016 Reinebrant H, Wixey J, Buller K. 2020. Hypoxia-ischemia in the immature rodent brain impairs
1017 serotonergic neuronal function in certain dorsal raphé nuclei. Neural Regen Res 15:457–
1018 463.
1019 Ren J, Friedmann D, Xiong J, Liu CD, Ferguson BR, Weerakkody T, DeLoach KE, Ran C,
1020 Pun A, Sun Y, Weissbourd B, Neve RL, Huguenard J, Horowitz MA, Luo L. 2018.
1021 Anatomically Defined and Functionally Distinct Dorsal Raphe Serotonin Sub-systems.
1022 Cell 175:472-487.e20.
1023 Ren J, Isakova A, Friedmann D, Zeng J, Grutzner SM, Pun A, Zhao GQ, Kolluru SS, Wang R,
1024 Lin R, Li P, Li A, Raymond JL, Luo Q, Luo M, Quake SR, Luo L. 2019. Single-cell
1025 transcriptomes and whole-brain projections of serotonin neurons in the mouse dorsal and
1026 median raphe nuclei. Elife 8.
1027 Risold PY. 2004. The Septal Region. In: The Rat Nervous System. Elsevier Inc. p 605–632.
1028 Rodríguez JJ, Noristani HN, Hoover WB, Linley SB, Vertes RP. 2011. Serotonergic
1029 projections and serotonin receptor expression in the reticular nucleus of the thalamus in
1030 the rat. Synapse 65:919–928.
1031 Schmidt EF, Kus L, Gong S, Heintz N. 2013. BAC Transgenic Mice and the GENSAT

1032 Database of Engineered Mouse Strains.

1033 Sourani D, Eitan R, Gordon N, Goelman G. 2012. The habenula couples the dopaminergic and
1034 the serotonergic systems: application to depression in Parkinson's disease. Eur J Neurosci
1035 36:2822–2829.

1036 Steinbusch HW. 1981. Distribution of serotonin-immunoreactivity in the central nervous
1037 system of the rat-cell bodies and terminals. Neuroscience 6:557–618.

1038 Storvik M, Tiihonen J, Haukijärvi T, Tupala E. 2007. Amygdala serotonin transporters in
1039 alcoholics measured by whole hemisphere autoradiography. Synapse 61:629–636.

1040 Su H-S, Bentivoglio M. 1990. Thalamic midline cell populations projecting to the nucleus
1041 accumbens, amygdala, and hippocampus in the rat. J Comp Neurol 297:582–593.

1042 Sur C, Betz H, Schloss P. 1996. Immunocytochemical detection of the serotonin transporter in
1043 rat brain. Neuroscience 73:217–31.

1044 Takumi T, Tamada K, Hatanaka F, Nakai N, Bolton PF. 2019. Behavioral neuroscience of
1045 autism. Neurosci Biobehav Rev 110:60–76.

1046 Tamada K, Takumi T. 2015. Serotonin disturbance in mouse models of autism spectrum
1047 disorders. In: Organism Models of Autism Spectrum Disorders. Springer New York. p
1048 239–262.

1049 Ternaux JP, Héry F, Bourgoin S, Adrien J, Glowinski J, Hamon M. 1977. The topographical
1050 distribution of serotoninergic terminals in the neostriatum of the rat and the caudate
1051 nucleus of the cat. Brain Res 121:311–326.

1052 Vallender EJ, Lynch L, Novak MA, Miller GM. 2009. Polymorphisms in the 3′ UTR of the
1053 serotonin transporter are associated with cognitive flexibility in rhesus macaques. Am J
1054 Med Genet Part B Neuropsychiatr Genet 150:467–475.

1055 Vertes RP. 2006. Interactions among the medial prefrontal cortex, hippocampus and midline
1056 thalamus in emotional and cognitive processing in the rat. Neuroscience 142:1–20.

1057 Vertes RP, Fortin WJ, Crane AM. 1999. Projections of the median raphe nucleus in the rat. J
1058 Comp Neurol 407:555–82.
1059 Vertes RP, Linley SB. 2008. Efferent and afferent connections of the dorsal and median raphe
1060 nuclei in the rat. In: Serotonin and Sleep: Molecular, Functional and Clinical Aspects.
1061 Birkhäuser Basel. p 69–102.
1062 Vitalis T, Cases O, Passemard S, Callebert J, Parnavelas JG. 2007. Embryonic depletion of
1063 serotonin affects cortical development. Eur J Neurosci 26:331–344.
1064 Warembourg M, Poulain P. 1985. Localization of serotonin in the hypothalamus and the
1065 mesencephalon of the guinea-pig. Cell Tissue Res 240:711–721.
1066 Weaver KJ, Paul IA, Lin RCS, Simpson KL. 2010. Neonatal Exposure to Citalopram
1067 Selectively Alters the Expression of the Serotonin Transporter in the Hippocampus: Dose-
1068 Dependent Effects. Anat Rec 293:1920–1932.
1069 Witter MP, Amaral DG. 2004. Hippocampal Formation. In: The Rat Nervous System. Elsevier.
1070 p 635–704.
1071 Xu Y, Sari Y, Zhou FC. 2004. Selective serotonin reuptake inhibitor disrupts organization of
1072 thalamocortical somatosensory barrels during development. Dev Brain Res 150:151–161.
1073 Zeng Z, Chen TB, Miller PJ, Dean D, Tang YS, Sur C, Williams DL. 2006. The serotonin
1074 transporter in rhesus monkey brain: comparison of DASB and citalopram binding sites.
1075 Nucl Med Biol 33:555–563.
1076

1077 **Figure Legends**

1078 **Figure 1: Innervation pattern of SERT-EGFP fibers across the rostro-caudal extent of**
1079 **thalamus.**

1080 *The terminal labelling density in each nucleus is written numerically within the brackets.*
1081 **(A-B)** *Sections from rostral thalamic pole* (**A)** PVT, CM nuclei and nucleus RE (6+). PT and
1082 AV nuclei (5+). AD (4+). AM and RT* nuclei (2+). ST nuclei (3+). SM and fx (0), fibers
1083 clustered at apex of SM (arrow head). *Rostral most RT was moderately labelled (fig not
1084 shown). **(B)** PVT, CM, RH nuclei and nucleus RE (6+). LD and AV nuclei (5+). IAM and AD
1085 nuclei (4+). AM and IAD nuclei (2+). VAL and RT nuclei (1+). MD and SMT nuclei (3+).
1086 MH (1+). **(C-D-E)** *Sections from mid thalamic level* **(C)** PVT, RH nuclei and nucleus RE (6+).
1087 IMD, LD, AV and CL nuclei (5+). CM, PCN and MD nuclei (3+), central part & dorsal area
1088 of MD (4+). VAL, VM, RT, SMT nuclei (1+), MH (3+ on ventral area, 1+ on dorsal). **(D)** PVT,
1089 RH nuclei, nucleus RE and SMT (6+). IMD, CL and LD nuclei (5+). MH, LH and MD nuclei
1090 (3+), central part & dorsal area of MD nuclei (4+). CM, PCN, PO, VAL, VPM, VPL, VM, and
1091 RT nuclei (1+) **(E)** PVT*, RE, SMT, LGd & LGv nuclei (6+). LP nuclei (5+). LD nuclei (4+).
1092 MH and LH (3+). MD nuclei (2+), less density on its ventral part. IMD and RH nuclei (3+).
1093 CM and RT nuclei (1+). PCN, CL, PO, VM, VAL, VPM, and VPL nuclei (<1). *Ascending
1094 fiber bundles traversing ahead via PAG were clustered as bilateral bundle in PVT (arrow head).
1095 Some of them divert laterally and in-between habenula. **(F-G)** *sections from the caudal*
1096 *thalamic pole* **F)** RE and LGd & LGv nuclei (6+), slightly less fibers on medial part of LGv.
1097 PVT nuclei (5+). LH and LP nuclei (4+). PF nuclei (1+; dorsal part, 2+). RT nuclei (1+). PO,
1098 VM, VPM and VPL nuclei (<1+). **G)** LGd & LGv nuclei (6+). LP (3+) nuclei. MG nuclei (2+)
1099 with slightly higher on lateral part. PO nuclei (1+).

1100 **Figure 2: Innervation pattern of SERT-EGFP fibers across the rostro-caudal extent of**
1101 **hypothalamus.**

(A-B) *Sections from preoptic hypothalamus* **(A)** LPO, MPO, MEPO nuclei (5+). AVPV nuclei (2+). Non-hypothalamic nuclei: SI (6+), which contains the collaterals of ascending pathway fibers detached from LPO area. MA nucleus and NDB (5+). Fibers from SI pass medially across the base of MA nucleus and NDB (yellow arrow). OT (5+). Fundus of striatum (FS) contains scattered collaterals of ascending fibers. **(B)** LPO area (6+). PVHap and PVpo nuclei (5+). MPN nuclei (4+). MPO area (4+) with 3+ density on its medial part. Non-hypothalamic nuclei: SI (6+). NDB (5+). MA nucleus (4+). OT (5+) with heavy clustering of fibers over its dorsal area. **(C-F)** *Sections from supraoptic hypothalamus* **(C)** LHA area (6+) with slightly less fibers on lateral part. AHN and ZI (5+). Fibers from LHA pass medially into the thalamus upon traversing through ZI or fx. SBPV, RCH and SO nucleus (3+). PVH; besides the part lining the ventricle (PVHpv; 5+), rest of the PVH is sparsely (1+) labelled. SCN (1+). Non-hypothalamic nuclei: SI (6+). **(D)** SCN; core (6+), shell (1+). Optic fibers entering into SCN were innervated by 5-HT fibers (arrow head). SBPV, PVi nuclei (5+). PVH (1+; except periventricular part, PVHpv 5+). **(E)** SCN (1+). SBPV area (5+). PVH nucleus (1+; except periventricular part, PVHpv 5+). **(F)** LHA (6+). AHN, ZI, RCH, PVH, SBPV, and PVi nuclei (5+). Fibers from LHA pass over supraoptic commissure to enter into the RCH (yellow arrow). Innervation in RCH decreases slightly on medial parts. Dorsally, fibers from LHA enter into the RE of thalamus and into ZI. SO nucleus (3+). Arc nuclei (2+). Non-hypothalamic area: SI (6+) **(G-H)** *Sections from supraoptic hypothalamus* **(G)** LHA (6+). DMHa, TU* nuclei and PVi (5+). VMH nuclei (5+; except dm part, 2+). Arc nucleus (1+). ZI (4+). *Collaterals of pathway fibers were observed to be directly passing into TU nuclei. **(H)** LHA (6+). VMH, TU, PH, STN nuclei, and PVi (5+). ZI (3+). DMH nucleus (2+). Arc nucleus (1+). Some fibers from LHA enter into the rostrally located GP through cpd. **(I-J-K)** *Sections from mamillary hypothalamus* **(I)** LHA (6+). PH and STN nuclei (5+). PMv and PMd (4+). TMd (2+). PVp (1+). ME (0). **(J)** LM* nucleus, and MMme (5+). LHA, MM nuclei, TMv (4+) and PH (3+). SUM (2+). PVp

(1+). *Collaterals of pathway fibers from VTA pass laterally to directly enter into the LM nuclei (black segmented arrow). **(K)** LM nucleus (5+). MM nucleus (4+) with mild (2+) innervation on medial part. SUM nucleus (1+)

Figure 3: Innervation pattern of SERT-EGFP fibers across the rostro-caudal extent of amygdala.

(A-B) *Rostral amygdalar section* **(A)** MEAad, medial part of AAA (6+). Lateral part of AAA, IA, BLA and BMAa nuclei (5+). CEA, NLOT*, and COAa (4+). *Rostral NLOT (5+) (figure not shown). Non amygdalar nuclei: EPd (6+) and EPv (5+). Fibers enter into the amygdala from LHA and SI (yellow arrow). **(B)** *BLAa, IA (6+). MEAad, and BMAa nuclei (5+). NLOT- layer 1&3 (4+), layer 2 (1+). CEA and BA nuclei (3+). COAa (2+). Non amygdalar nuclei: EPd (6+) EPv (5+). * BLAa was bounded by very dense clustered fibers within the external capsule on medial and ventral side. **(C-D)** *Mid amygdalar section* **(C)** BLAa (6+). MEAad, and IA nuclei (5+). LA, CEA, MEAav, BMAp, COApl, and PAA (3+). Fibers travelling within stria terminalis (st) project into the CEA and MEAad nuclei. **(D)** BLAa and BLAp (6+). BLAv nucleus (5+). BMAp nucleus (4+), shows the intranuclear gradient. LA, CEA, MEApd, MEAav, COApm, COApl, and PAA (3+). Fibers travelling within stria terminalis (st) project into the CEA and MEApd nuclei. **(E-F)** *Caudal amygdalar section* **(E)** BLAp nuclei (6+). BLAa, BLAv, BMAp, COA, and PAA (5+). MEApd, MEApv, and LA nuclei (3+). Stria terminalis (st) was very densely (6+) clustered with SERT-EGFP fibers both in (E) and (F). **(F)** BLAp nuclei (6+). PA, BLAv, COA (pm,pl), and PAA (5+). BMAp nucleus (3+). Transition zone (TR) between PAA and PIR was mildly (2+) innervated.

Figure 4: Innervation pattern of SERT-EGFP fibers across the rostro-caudal extent of septal nuclei.

(A-B) *Sections from rostral septal level* **(A)** LSr nuclei (6+), collaterals of pathway fibers travelled through LSr to form the supracallosal bundle (scb) located above the CC (arrow head).

NDB (4+). SH nuclei (2+). IG contains the collaterals of pathway fibers which innervate the medial cortex. Non-septal nuclei: TTd (3+) **(B)** NDB, MS, and LSr nuclei (5+). Ventrodorsally running collaterals of pathway fibers were clustered very densely (6+) in the medial and lateral border of MS which terminated by bounding the SH nuclei dorsally. SH nuclei (1+). **(C-D)** *Sections from mid septal level.* LSr nuclei (5+). NDB and medial part of MS (3+). Fibers can be observed entering into the septum via SI. Ventrodorsally running collaterals of pathway fibers clustered very densely (6+) in the lateral border of MS which reached upto the ventral border of CC. **(C)** LSc (3+) with vertically oriented fibers abutting the CC (arrow head). Islm (0) **(D)** LSc (2+) with vertical fibers abutting CC (black arrow head). Very dense (6+) cluster of fibers between LSr and NAc (yellow arrow head). Islm (5+). **(E-F)** *Sections from caudal septal level.* **(E)** Medially diverted collaterals of ascending fibers from LPO nuclei entered into the septum. LSr nuclei (4+). Mediolaterally, directed fibers in LSr. LSv nuclei (3+), except densely clustered fibers at its dorsal part (arrow). LSc (1+) with vertical fibers at the dorsal border. Column of fornix (fx) (0). Thin fascicle of fiber passing ventrodorsally in between the two columns. **(F)** SF nuclei (4+); mediolaterally oriented fibers. LSc nuclei (1+) with vertical fibers at its dorsal border (arrow head). TRS (1+). LSv nucleus (3+).

Figure 5: Innervation pattern of SERT-EGFP fibers across the rostro-caudal extent of caudoputamen and nucleus accumbens.

(The images are the serial sections arranged rostro-caudally) **(A)** CP (2+). NAc (4+). Fibers entered into the CP and NAc through collaterals of fibers running in external capsule (arrow head) (A-C). **(B)** CP (3+ on lateral area and 2+ on medio-dorsal part). Fibers running within external capsule (arrow head) wind up around olfactory limb of anterior commissure (aco) or directly enter into the CP and NAc (3+). **(C)** collaterals of pathway fibers within SI wind around aco to enter into the medial side of CP (segmented black arrow line). Medial part (3+) have higher innervation compared to lateral (2+). Region of thalamocortical fibers traversing

1177 through CP appear as circular gap (green arrow head). Collaterals of ascending pathway fibers
1178 appear as patch in CP (red arrow head) and NAc (blue arrow head). NAc (2+), in the area
1179 except the patch (blue arrow head) **(D)** CP (3+ homogeneous distribution throughout). GPe
1180 (6+). Empty holes in the CP and GPe are areas of non-labelled thalamocortical fibers.
1181 Collaterals of pathway fibers in the SI, directly innervated the GPe. **(E)** CP (4+). GPe (6+).
1182 Fibers arising from main ascending bundle at LHA entering into the GPe through SI. Fibers
1183 were very densely clustered only around the thalamocortical fibers (whorl like pattern) in the
1184 GPi and sparse elsewhere. **(F)** *Sagittal section showing both caudoputamen and nucleus*
1185 *accumbens*. Gap indicates unlabeled thalamocortical fibers. Thin, relatively straight fibers were
1186 seen terminating mainly in the NAc (red arrow head) and few in the CP. Some of them entered
1187 into the external capsule (yellow arrow head) which provided the innervation both to the cortex
1188 and CP. **(G)** enlarged view of nucleus NAc showing the straight, non-varicose terminal fibers
1189 seen in E (red arrow head)

1190 **Figure 6: Innervation pattern of SERT-EGFP fibers across the rostro-caudal extent of**
1191 **bed nuclei of stria terminalis and olfactory tubercle.**

1192 *(The images are the serial sections arranged rostro-caudally)* **A-B:** *anterior BNST*. Fibers
1193 entered into the BNST via collaterals of pathway fibers clustered within SI. **(A)** am and al
1194 nuclei (4+). **(B)** am and al nuclei (5+). ov and fu nuclei (2+). **C-D:** *posterior BNST*. **(C)** am and
1195 al nuclei (6+). dm, mg, v, and rh nuclei (5+). Pr nuclei (2+), except at ventral area. Fibers on
1196 pr, am, al and rh nuclei entered into the stria terminalis (st). **(D)** tr nuclei (6+). if, v, al nuclei
1197 (5+). pr nuclei (2+). Fibers from BNST entered into the stria terminalis (st) to run dorsally
1198 above the thalamus. (**A-B)** OT (6+). Fibers in OT were clustered around isl; while latter were
1199 almost devoid of labelling. (**C-D)** OT (5+); fibers distributed were fine in morphology and
1200 homogeneously distributed throughout.

Figure 7: Innervation pattern of SERT-EGFP fibers across the rostro-caudal extent of hippocampus

(A) *Rostral end of the dorsal hippocampus*. Fibers entered into the hippocampus through dorsal fornix (df) and fimbria (fi). Some of these collaterals passed into the alveus (alv) and ramified into the SO. SO and SR (4+). SP, PO and MO layer (1+). SG (0). **(B-C)** SO and SR of CA1 and CA2 zone of HPF (3+). SO and SR of CA3 zone of HPF (4+). Whole extent of SLM (5+). Whole extent of SP (1+). Dorsal part of MO layer of DG (3+). Ventral part of MO layer of DG and PO (1+). SG (0). Fibers enter into the hippocampus through fimbria (fi) and fibers spreading laterally from SLM made the CA3 SO and CA3 SR appear more clustered with fibers respectively. **(C)** *Retrosplenial part of dorsal hypothalamus***.** Collaterals of pathway fiber from supracallosal bundle (scb) passed ventrally into the hippocampus (black arrow) mainly into the alvelus (alv) and SLM. **(D)*** *Ventral hippocampus*. SO, SR of CA1 (3+). SLM (6+). MO layer (3+) except at apex. SR of CA3 (5+). SO of CA3 (3+). SP and PO (1+). SG (0). SUBv and SUBd (3+). Fibers passing through the SLM moved out laterally to innervate the rhinal cortex. **(E)** *Image showing the sources of innervation fibers of the hippocampus.* supracallosal bundle (scb) running dorsally above corpus callosum (CC) wind around the splenium to enter the hippocampus (yellow arrow head). Collaterals of pathway fibers enter into the septal nuclei run dorso-caudally to pass into the dorsal fornix (df) and fimbria (black arrow) which subsequently innervate the hippocampus.

(D)** ***Image showing both the ventral hippocampus and cortical section from occipital pole. *RSP, Visual and auditory cortex*: layer 1 (4+), layer 2/3 and 4 (1+), underlying layers (2+). *Temporal association area (TEa)* (3+). *Rhinal cortex*: 6+ except in second and deepest layer**.**

Figure 8: Innervation pattern of SERT-EGFP fibers across the rostro-caudal extent of cortex.

1225 *(The images are serial cortical sections arranged rostro-caudally)* **(A)** *Rostral pole of the*
1226 *cortex*. Layer 1 in all the areas (5+). *PL area:* patch like cluster of fibers. layer 2 and 2/3 (4+).
1227 rest of the layers (3+). *ACAd area* (3+). *MOs area:* layer (5+) and deeper part of 6a (4+), other
1228 layers (3+). *MOp area and AId area:* layer 5 (5+), rest of the layers (3+). *ORB area:* layer 5
1229 (4+) and rest of the layers (3+) **(B)** Layer 1 in all areas (5+). *ILA, PL, and ACAd area* (3+).
1230 Fibers from endopiriform nuclei (EPd) enter into the medial cortex through the deeper layer of
1231 ILA and PL cortex. *MOs area:* 3+ in rest of the layers except 6b (2+). *MOp area:* Layer 5 (4+).
1232 Rest of the layers (3+). *SSp, GU and AI area:* layer 5 and 6b (5+). Layer 6a (3+). Layer 2/3
1233 (2+). *ORB area:* 2+ in rest of the layers except layer 5 (3+). Fibers enter into the layer 1 of
1234 lateral cortex through areas around rhinal fissure. **(C)** Layer 1 in all areas (5+). *ILA, PL and*
1235 *ACAd area* (3+) in rest of the layers. Fibers enter into this medial cortex via medial forebrain
1236 bundle (mfb) (black arrow line) and indusium griseum (ig) (yellow arrow head). *MOs and Mop*
1237 *area:* layer 5 and 6a (3+). 2+ in rest of the layers. *SSp area:* Layer 5 and 6b (5+). Fibers
1238 clustered within the claustrum (CLA) distribute to layer 6a (3+). Layer 2/3 and 4 (2+). *GU and*
1239 *AI area:* layer 5 (4+). Rest of the layers (3+). Fibers clustered within EPd enter into the lateral
1240 cortex mainly through the layer 1 and Layer 5. **(D)** Layer 1 in all areas (5+). *ACAv and ACAd*
1241 (2+) except at the deeper layers where fibers from supracallosal bundle (scb, arrow head) pass
1242 dorsally towards the motor areas and horizontally into layer 6b. *MOs and MOp* area (3+) in
1243 upper layers; 2+ in deeper layers 6a and 6b. *SS area:* layer 5 (5+). Layer 6a and 6b in the barrel
1244 field (bf) area (4+). Rest of layer 6 including layer 2/3 (2+). Barrel field area in the SS cortex
1245 receive higher projections compared to rest of the layers. *Visceral area (VISC), GU and AIp*
1246 *area:* Fibers from EPd traverse into the lateral cortex through the layer 1, 5 and 6b (5+ in all
1247 of these layers) of these areas. Fibers travelling through external capsule (ec, arrow head) also
1248 provide innervation to deeper cortical layers and caudoputamen. *Piriform cortex (PIR):* 3+ in
1249 all of the layers without laminar pattern. **(E)** Layer 1 in all areas (5+). *RSP area* (3+). A vertical

band of fibers between layer 2 and 2/3. Fibers from supracallosal bundle (scb, arrow head) pass dorsally towards the motor areas. *Motor areas (MOs and MOp):* layer 5 (4+) and rest of the layers (3+). *Somatosensory area (SSs and SSp):* layer 5 (4+) and rest of the layers (2+). **(F)** Layer 1 in all areas (5+). *Retrosplenial area:* RSPagl (3+). RSPv and RSPd (2+). *Visual area:* deeper layers (6a, 6b) (3+). Upper layers (1+). *Auditory area:* layer 5 and below (4+). Layer 2/3 and 4 (1+). *Rhinal and temporal association area (TEa):* 5+ in rest of the layers except layer 2/3 (2+). *Piriform cortex (PIR):* laminar pattern, layer 1 (5+), deeper layers (3+). **(G)** Layer 1 in all areas (5+). *Retrosplenial cortex (RSP)* (2+). *Visual and auditory area* (1+)**.** *Rhinal and temporal association area (TEa):* 5+ in rest of the layer except layer 2/3**. (H)** *Sagittal cortical section* showing the dense cluster of collateral pathway fibers in the induseum griseum (IG) (arrow head) which is one of the main sources of innervation to the medial cortex.

Figure 9: Innervation pattern of SERT-EGFP fibers in the olfactory bulb.

(A) SERT-EGFP fibers arrangement in the main olfactory bulb (MOB) exhibit the laminar pattern. GL (5+). OPL (1+). MI, IPL and GR layer (4+). OV (1+). Optic nerve layer (onl) (0). **(B)** Accessory olfactory bulb (AOB). GR layer (1+). MI and GL layer (0). Anterior olfactory nuclei (AON) acted as the route for passage for the collaterals of ascending fibers reaching to MOB

Figure 10. Innervation pattern of SERT-EGFP fibers in the cerebellum.

Sparsely (1+) labelled layers of the cerebellum. Outermost molecular layer (MO) and white matter (WM) tree almost appear scanty. Fibers are mainly distributed in the pyramidal (py, arrow head) or granular (gr) layer. Moderate (3+) labelling within the deep cerebellar nuclei (IP and FN). Fibers from raphe nuclei passed dorsally directly into the deep nuclei.

Table 2 Innervation density across different brain areas and their sub-divisions

Brain areas and their subdivisions	Innervation density change rostro-caudally
THALAMUS	
Midline nuclei	
Paraventricular Thalamic nucleus (PVT)	6+ to 5+

Paratenial nucleus (PT)	5+
Rhomboid nucleus (RH)	6+ to 3+
Nucleus reuniens (RE)	6+
Intralaminar nuclei	
Central lateral nucleus (CL)	5+ to 1+
Paracentral nucleus (PC)	3+ to 0
Central medial nucleus (CM)	6+ to 1+ to 2+
Parafascicular nucleus (PF)	2+ (dorsal), 1+ (ventral) (intranuclear gradient)
Association nuclei	
Mediodorsal nucleus (MD)	3+ to 2+ (4+ on dorsal and central part)
Intermediodorsal nucleus (IMD)	5+ to 3+
Submedial thalamic nucleus (SMT)	3+ to 1+ to 6+
Anterodorsal nucleus (AD),	4+
Anteroventral nucleus (AV)	5+
Anteromedial nucleus (AM)	2+
Interanteromedial nucleus (IAM)	4+ to 2+
Lateral dorsal nucleus (LD)	5+ to 4+
Lateral posterior nucleus (LP)	5+ to 4+
Inter anterodorsal nucleus (IAD)	2+
Principal nuclei	
Ventral posteromedial nucleus (VPM)	< 1+
Ventral posterolateral nucleus (VPL)	< 1+
Ventroanterior lateral complex (VAL)	< 1+
Ventromedial nucleus (VM)	< 1+
Posterior nucleus (PO)	1+ to <1
Lateral geniculate nucleus (LG)	6+
Medial geniculate nucleus (MG)	2+
Epithalamus	
Medial habenula	1+ to 3+ (intranuclear gradient)
Lateral habenula	3+ to 4+
Reticular nucleus	3+ to 1+
Other areas	
fasciculus retroflexus (fr)	0
mamillotegmental tract (mmt)	0
posterior commissure (pc)	0
internal capsule (ic)	0
cerebral peduncle (cpd)	0 (fibers traversing through at some level)
Internal capsule (int)	0
stria medullaris (sm)	0 (fibers clustered at dorsal part)
stria terminalis (st)	(3+) (fibers passing through)
HYPOTHALAMUS	
Preoptic region	
Median preoptic nucleus (MEPO)	5+
Medial preoptic area (MPO)	5+ to 4+ (3+ on medial part)
Anteroventral periventricular nuclei (AVPV)	2+
Medial preoptic nucleus (MPN)	4+
Lateral Preoptic nucleus (LPO)	Route for the ascending forebrain bundle
Supraoptic region	
Supraoptic nucleus (SO)	3+
Retrochiasmatic nucleus (RCN)	4+ to 5+
Anterior hypothalamic nucleus (AHN)	5+
Suprachiasmatic nucleus (SCN)	1+ to 6+ (intranuclear gradient at midlevel)
Subparaventricular zone (SBPV)	3+ to 5+
Lateral hypothalamic area (LHA)	Route for the ascending forebrain bundle
Paraventricular hypothalamic nucleus (PVH)	

Periventricular part (PVHpv)	5+
Rest of other areas	1+ to 5+
Tuberal region	
Ventromedial hypothalamic nucleus (VMH) (except dorsomedial part)	5+ (dorsomedial part 2+)
Dorsomedial hypothalamic nucleus (DMH)	5+ to 2+
Arcuate hypothalamic nucleus (ARH)	1+
Tuberal nucleus (TU)	5+
Mamillary region	
Posterior Hypothalamic nucleus (PH)	5+ to 1+
Posterior part of periventricular nucleus (PVp)	1+
Premamillary mamillary nucleus, ventral (PMv) & dorsal (PMd)	4+
Lateral mamillary nucleus (LM)	5+
Tuberomammillary mamillary nucleus, dorsal (TMd) & ventral (TMv)	2+ and 4+
Medial mamillary nucleus (MM)	4+ (intranuclear gradient posteriorly)
Median part of MM (MMme)	5+
Supramamillary nucleus (SUM)	2+ to 1+
Median eminence (ME)	0
Zona incerta (ZI)	5+ to 1+
Subthalamic nucleus	5+
Periventricular nucleus (PV); preoptic (Pvpo), anterior (Pva) and intermediate (Pvi) part	5+
Other areas	
Optic tract (opt)	0
Fornix (fx)	0
Fasciculus retroflexus (fr)	0
Mamillotegmental tract (mtt)	0
Cerebral peduncle (cpd)	0 (at some level fibers traverse through it)
Anterior commissure (aco)	0
Substantia Innominata (SI)	6+
Magnocellular Nuclei (MA)	5+ to 4+ (heavy fibers at its ventral part)
Nucleus of diagonal band (NDB)	5+
AMYGDALA	
Deep or basolateral group	
Lateral amygdalar nucleus (LA)	3+
Basolateral amygdalar nucleus (BLA)	
Anterior (BLAa)	6+ to 5+
Posterior (BLAp)	6+
Ventral part (BLAv)	5+
Basomedial amygdalar nucleus (BMA)	
Anterior part (BMAa)	5+
Posterior part (BMAp)	3+ to 5+ to 3+
Superficial or cortical-like group	
Nucleus of lateral olfactory tract (NLOT)	5+ to 4+ (laminar)
Bed nucleus of accessory olfactory tract (BA)	3+
Cortical amygdalar nucleus	2+ to 5+
Anterior (CoAa)	4+ to 2+
Posterior (CoAp)	3+ to 5+
Piriform-amygdaloid area (PAA)	3+ to 5+
Centromedial group	
Medial amygdalar nuclei (MeA)	
Anterodorsal part (MEAad)	6+ to 5+
Anteroventral part (MEAav)	3+

Posteroventral part (MEApv)	3+
Posterodorsal part (MEApd)	3+
Central amygdalar nuclei (CeA)	4+ to 3+
Other nuclei	
Anterior amygdalar area (AAA)	5+ (6+ on its medial parts)
Intercalated cell masses (IC)	6+ to 5+
Posterior amygdaloid nucleus (PA)	5+
Non amygdalar nuclei	
Endopiriform nuclei; dorsal (EPd) and ventral (EPv)	6+ and 5+ respectively
SEPTUM	
Nucleus of diagonal band (NDB)	5+ to 3+
Medial septum (MS)	5+ to 3+ (6+ at its limiting zone with LS)
Lateral septal nucleus (LS)	
Caudal part (LSc)	3+ to 1+
Rostral part (LSr)	6+ to 5+ to 4+
Ventral part (LSv)	3+ (except the dorsal edge)
Other Septal areas	
Septo-hippocampal nucleus (SH)	1+
Insula magna (islm)	0 to 5+
Triangular septal nucleus (TRS)	1+
Septofimbrial nuclei (SF)	4+
Column of fornix (fr)	0
Anterior commissure, olfactory (aco) and temporal (act) limb	0
BASAL GANGLIA	
Caudoputamen (CP)	2+ to 3+ to 4+
Globus pallidus (GP)	6+ (whorl in internal segment)
NUCLEUS ACCUMBES (NAc)	4+ to 3+
Other areas	
Corpus callosum (CC)	0
BED NUCLEI OF STRIA TERMINALIS	
Anterior division of BNST	
Anteromedial (Am) area	4+ to 5+
Anterolateral (Al) area	4+ to 5+
Oval nucleus (Ov)	2+
Fusiform nucleus (Fu)	2+
Posterior division of BNST	
Principal nucleus (Pr)	2+ (fibers clustered at ventral area)
Dorsomedial nucleus (Dm)	5+
Rhomboid nucleus (Rh)	5+
Magnocellular nucleus (mg)	5+
Ventral nucleus (V)	5+
Interfascicular nucleus (If)	5+
Transverse nucleus (Tr)	6+
Anteromedial (Am) and Anterolateral (Al) area	6+
HIPPOCAMPUS	
Hippocampal formation (HPF)	
stratum oriens (SO)	3+ (CA3 SO: 4+)
pyramidal layer (Py)	1+
stratum radiatum (SR)	3+ (CA3 SR: 4+) (CA3 SR of ventral HPF: 5+)
stratum lacunosum moleculare (SLM)	5+ (slm of ventral hippocampus: 6+)
Dentate gyrus (DG)	
molecular layer (Mo)	3+ (dorsal layer), 2+ (ventral layer)
granule cell layer (SG)	0

polymorph layer (Po)	1+
Subiculum (SUB)	3+
CORTEX	
Prefrontal cortex	
Prelimbic area (PL)	Patch like fiber cluster in upper layers in 4+ density (rostral pole) to 3+ density (caudal pole); except 5+ density in layer 1
Infralimbic area (IL)	3+ density rostro-caudally, except 5+ density in layer 1
Anterior cingulate area (ACA)	3+ density rostro-caudally, except 5+ density in layer 1
Agranular insular cortex (AI)	5+ density in layer 1 and 5 (rostral pole) to 5+ density in layer 1, 5 and 6b (caudal pole)
Retrosplenial cortex	3+ density (rostral pole) slight decrease in density caudally
Motor cortex	5+ density in layer 1 5+ to 4+ density change in layer 5 rostro-caudally 3+ density in other layers
Somatosensory cortex	5+ density in layer 1 5+ to 4+ density change in layer 5 3+ to 2+ density change in other layers
Barrel field area	5+ density except at layer 2/3
Auditory and Visual cortices	5+ to 4+ density change in layer 1 1+ density in layer 2/3 and 4 3+ to 2+ density change in other layers
Rhinal area	2+ density in layer 2/3 (rostro-caudally) and the deepest layer of caudal rhinal area 5+ to 6+ density change in other layers
Piriform cortex	3+ density at rostral pole (no laminar pattern) 5+ density at layer 1 and 3+ in underlying layers at caudal pole
OLFACTORY BULB	
Main Olfactory Bulb (MOB)	
Glomerular layer (Gl)	5+
Outer plexiform layer (OPL)	1+
Mitral layer (Mi)	4+
Internal plexiform layer (IPL)	4+
Granule layer (Gr)	4+
Olfactory ventricle (OV)	1+
Olfactory nerve layer (ONL)	0
Accessory Olfactory Bulb (AOB)	
Glomerular layer (gr)	0
Mitral layer (MI)	0
Granule layer (gr)	1+
Anterior olfactory nuclei (AON)	5+
Olfactory tubercle (OT)	5+
Island of Calleja (isl)	0
CEREBELLUM	
Purkinje cell layer and granular cell layer	1+
Molecular cell layer and white matter	0
Deep cerebellar nuclei	3+

1273

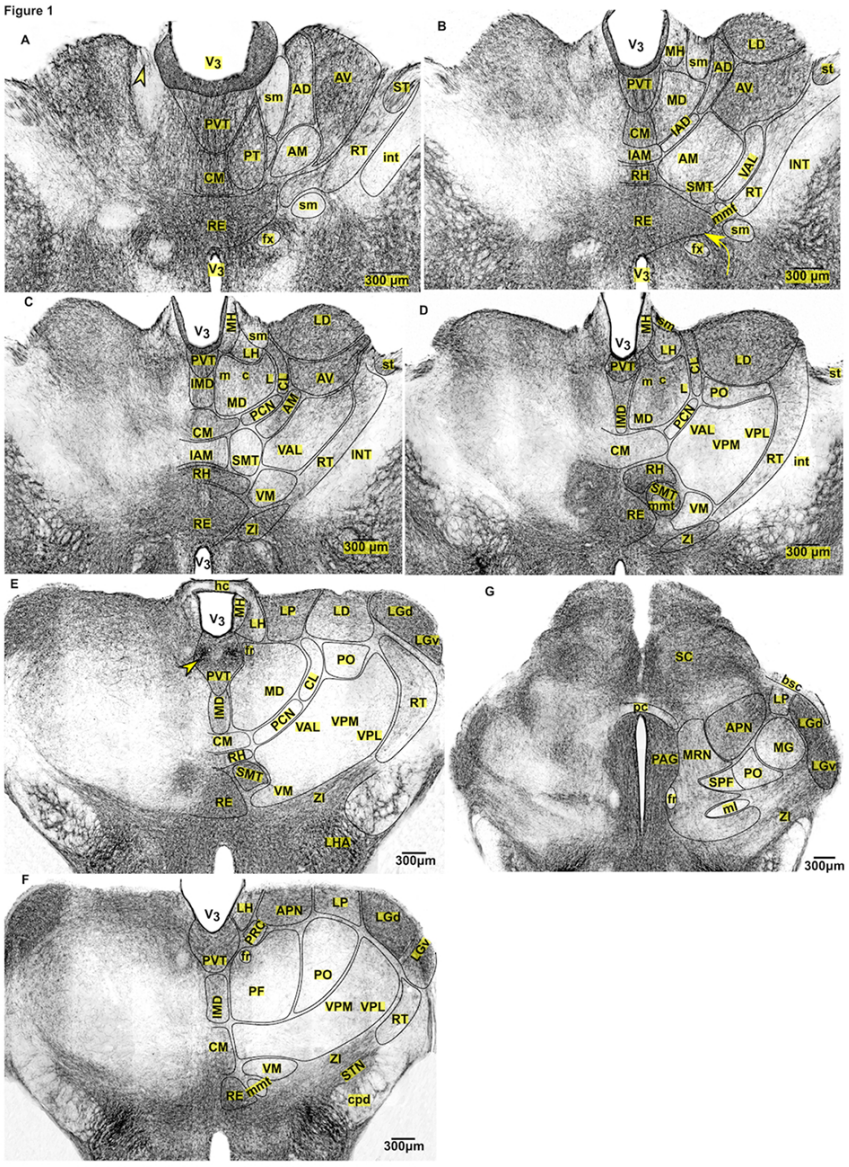
Figure 1
A
V3
AD
AV
ST
sm
PVT
PT
AM
RT
int
CM
sm
RE
fx
V3
300 µm
B
V3
MH
sm
LD
st
PVT
MD
AV
AD
CM
IAD
IAM
AM
VAL
INT
RH
SMT
RT
RE
mmt
sm
fx
V3
300 µm
C
V3
MH
sm
LD
LH
PVT
st
m
c
L
CL
IMD
AV
MD
PCN
AM
CM
IAM
SMT
VAL
RT
INT
RH
VM
RE
ZI
300 µm
V3
D
V3
MH
sm
LH
PVT
CL
LD
st
m
c
L
PO
IMD
MD
PCN
VAL
VPL
CM
VPM
RT
int
RH
SMT
mmt
VM
RE
ZI
300 µm
E
hc
V3
MH
LH
LP
LD
LGd
LGv
fr
PO
PVT
MD
CL
IMD
RT
PCN
VAL
VPM
VPL
CM
RH
SMT
VM
ZI
RE
LHA
300µm
G
SC
bsc
pc
LP
APN
LGd
PAG
MRN
MG
LGv
SPF
PO
fr
ml
ZI
300µm
F
V3
LH
APN
LP
LGd
PRC
LGv
PVT
fr
PO
PF
IMD
VPM
VPL
RT
CM
VM
ZI
STN
RE
mml
cpd
300µm

Fig. 1

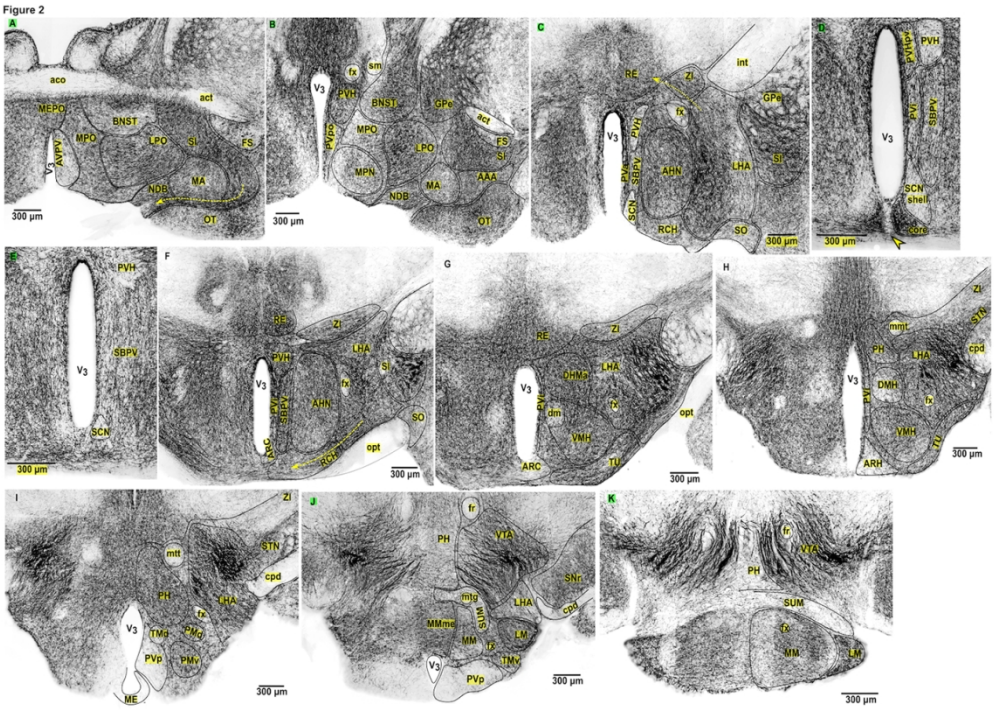
Figure 2
A
aco
act
MEPO
BNST
MPO
LPO
SI
FS
PaAP
V3
NDB
MA
OT
300 µm
B
fx
sm
V3
PVH
BNST
GPe
acr
MPO
LPO
FS
SI
MPN
AAA
NDB
MA
OT
300 µm
C
RE
ZI
int
GPe
fx
V3
PVH
PaMP
SBPV
AHN
LHA
SI
SCN
RCH
SO
300 µm
D
PVH
PaMP
SBPV
V3
SCN
shell
core
300 µm
E
PVH
SBPV
V3
SCN
300 µm
F
RE
ZI
LHA
PVH
SI
V3
fx
PaMP
SBPV
AHN
SO
SCN
RCH
opt
300 µm
G
RE
ZI
V3
DHMa
LHA
PaMP
dm
fx
opt
VMH
ARC
TU
300 µm
H
ZI
mmt
STN
PH
LHA
cpd
V3
PaMP
DMH
fx
YMH
TU
ARH
300 µm
I
ZI
mtt
STN
cpd
PH
LHA
fx
V3
TMd
PMd
PVp
PMv
ME
300 µm
J
fr
PH
VTA
SNr
mtg
LHA
cpd
MMme
MMl
MM
LM
rf
V3
TMv
PVp
300 µm
K
fr
VTA
PH
SUM
fx
MM
LM
300 µm

Fig. 2

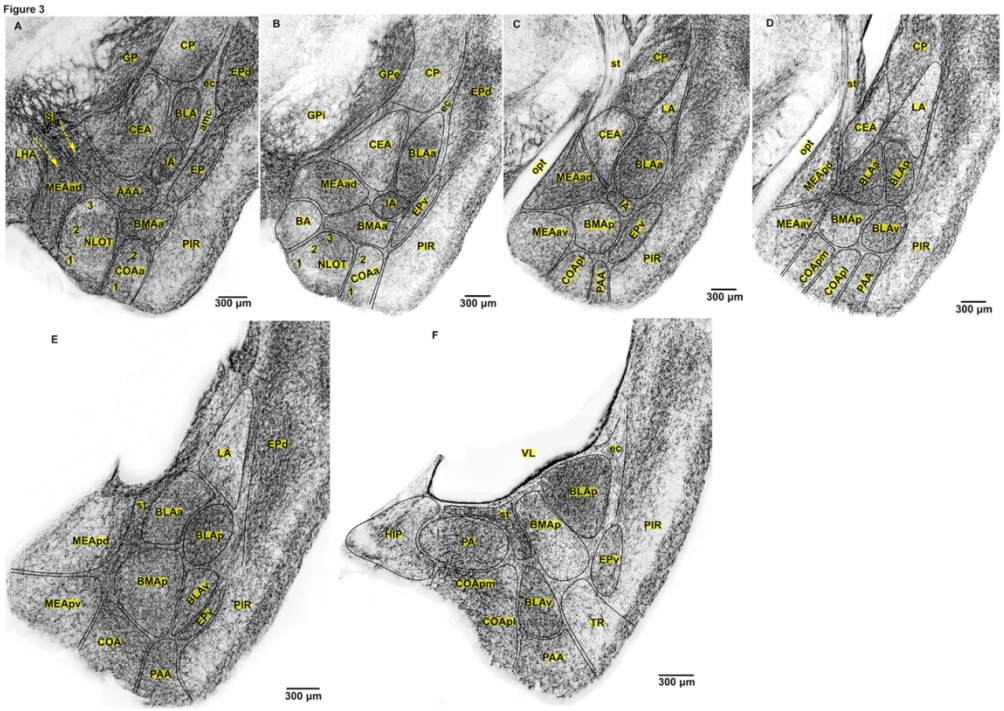
Figure 3
A
GP
CP
EPd
ac
BLA
CEA
LHA
IA
EP
MEAad
AAA
3
2
BMAa
NLOT
PIR
1
2
COAa
1
300 µm
B
GPe
CP
GPi
ac
EPd
CEA
BLAa
MEAad
IA
EPv
BA
BMAa
3
2
1
NLOT
2
COAa
PIR
1
300 µm
C
st
CP
LA
CEA
opt
MEAad
BLAa
IA
MEAav
BMAp
EPv
COApl
PAA
PIR
300 µm
D
st
CP
LA
CEA
opt
MEApm
BLAa
BLAp
MEAav
BMAp
BLAv
PIR
COApm
COApl
PAA
300 µm
E
LA
EPd
BLAa
BLAp
MEApd
BMAp
BLAa
MEApv
EPv
PIR
COA
PAA
300 µm
F
VL
ac
BLAp
st
HIP
PA
BMAp
PIR
EPv
COApm
BLAv
COApl
TR
PAA
300 µm

Fig. 3

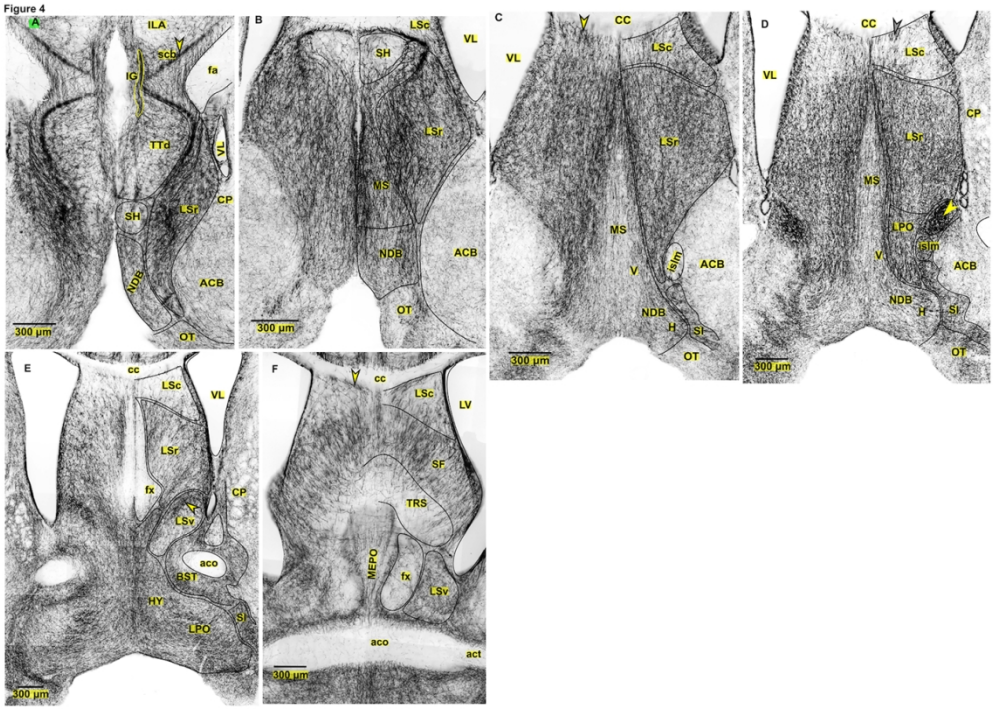
Figure 4
A
ILA
scb
IG
fa
TTd
VL
CP
SH
LSr
NDB
ACB
OT
300 µm
B
LSc
VL
SH
LSr
MS
NDB
ACB
OT
300 µm
C
CC
LSc
VL
LSr
MS
V
islm
ACB
NDB
H
SI
OT
300 µm
D
CC
LSc
VL
CP
LSr
MS
LPO
V
islm
ACB
NDB
H
SI
OT
300 µm
E
cc
LSc
VL
LSr
fx
CP
LSv
aco
BST
HY
LPO
SI
300 µm
F
cc
LSc
LV
SF
TRS
MEPO
fx
LSv
aco
act
300 µm

Fig. 4

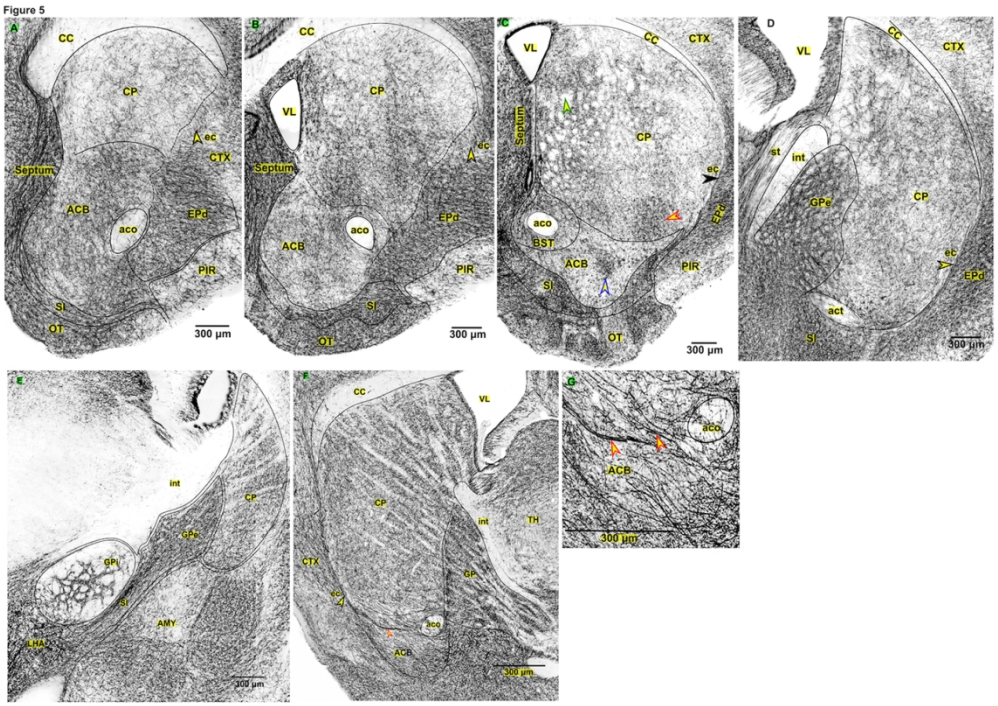
Figure 5
A
CC
CP
ec
CTX
Septum
ACB
aco
EPd
PIR
SI
OT
300 µm
B
CC
CP
VL
ec
Septum
ACB
aco
EPd
PIR
SI
OT
300 µm
C
VL
CC
CTX
Septum
CP
ec
aco
BST
ACB
PIR
SI
OT
300 µm
D
VL
CC
CTX
st
int
GPe
CP
ec
EPd
act
SI
300 µm
E
int
CP
GPe
GPi
SI
AMY
LHA
300 µm
F
CC
VL
CP
int
TH
CTX
GP
ec
aco
ACB
300 µm
G
aco
ACB
300 µm

Fig. 5

Figure 6

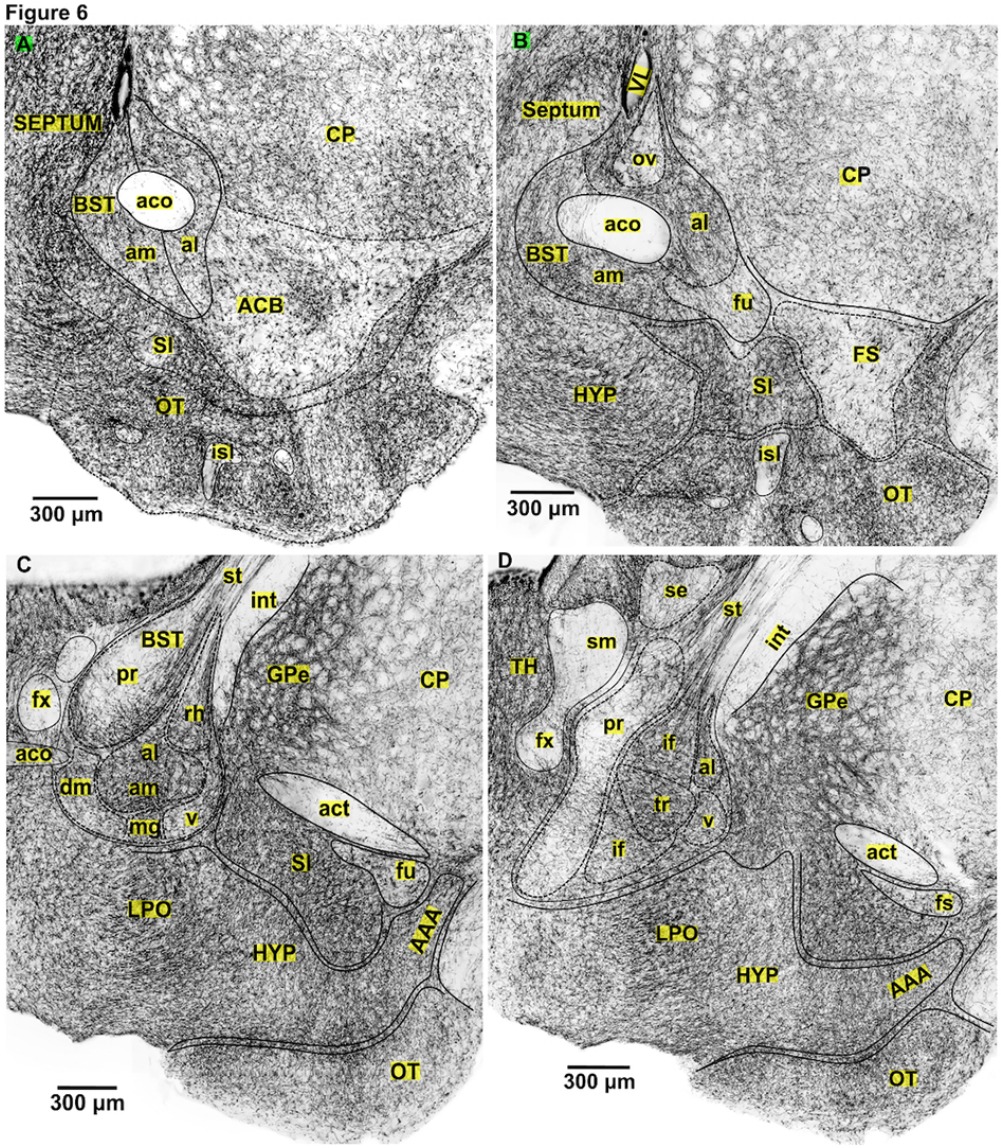

Fig. 6

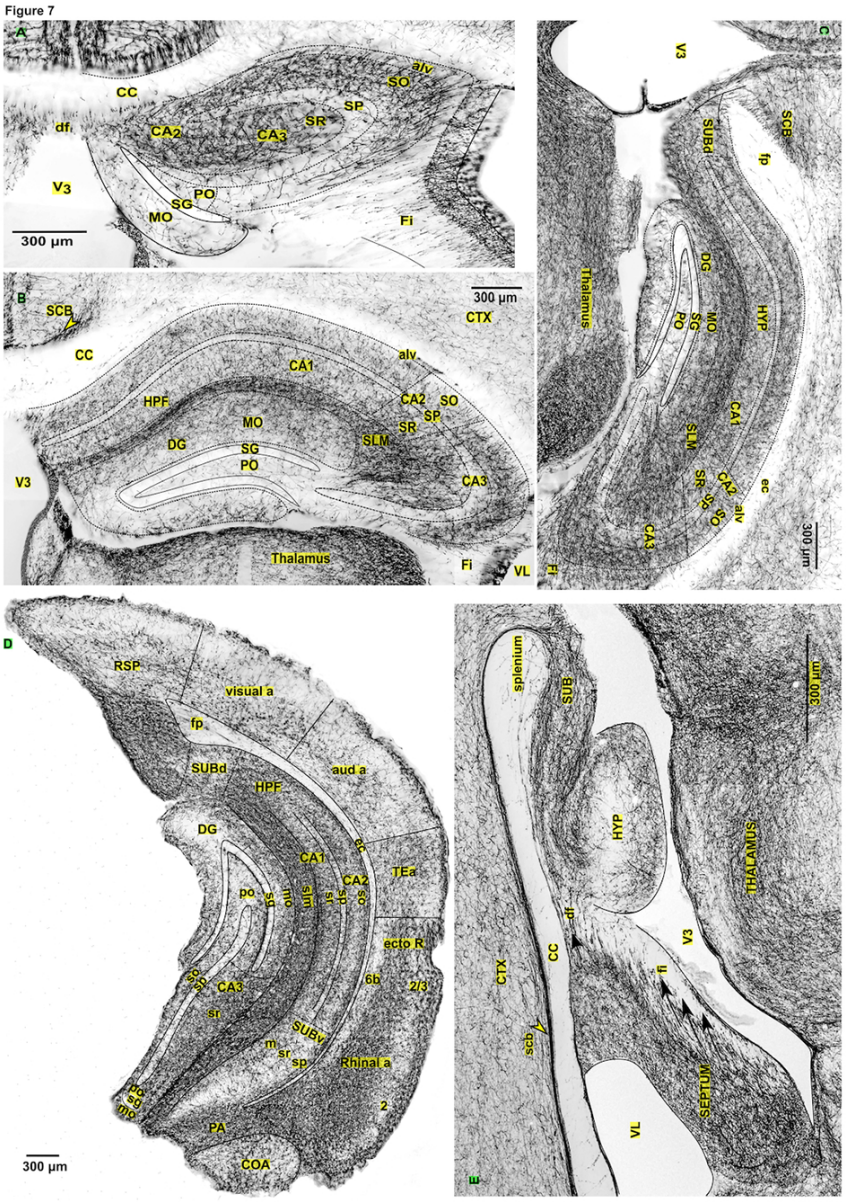
Figure 7
A
alv
SO
CC
SP
SR
df
CA2
CA3
V3
PO
SG
MO
Fi
300 µm
B
SCB
300 µm
CTX
CC
CA1
alv
HPF
CA2
SO
SP
MO
SR
DG
SLM
SG
PO
V3
CA3
Thalamus
Fi
VL
C
V3
SUBd
SCB
fp
DG
Thalamus
HYP
MO
SG
PO
CA1
SLM
SR
CA2
SO
alv
ec
CA3
300 µm
fi
D
RSP
visual a
fp
SUBd
aud a
HPF
DG
CA1
TEa
ecto R
6b
2/3
CA3
SUBv
Rhinal a
2
PA
COA
300 µm
splenium
SUB
300 µm
HYP
THALAMUS
df
V3
CC
CTX
fi
scb
SEPTUM
VL
m

Fig. 7

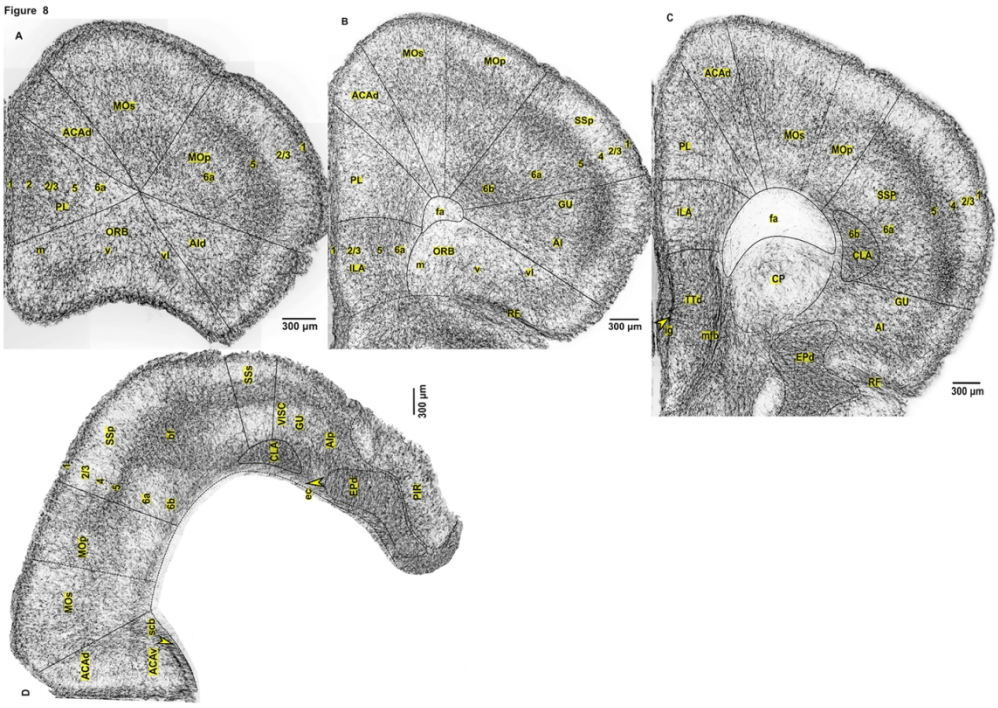
Figure 8
A
MOs
ACAd
MOp
6a
5
2/3
1
2
PL
ORB
m
v
vl
AId
300 µm
B
MOs
MOp
ACAd
SSp
4
2/3
1
5
PL
6a
6b
fa
GU
ORB
2/3
5
6a
ILA
m
v
vl
AI
RF
300 µm
C
ACAd
PL
MOs
MOp
ILA
fa
SSp
4
2/3
1
5
6b
6a
CLA
CP
GU
AI
EPd
RF
300 µm
D
SSs
SSp
bfd
VISC
GU
CLA
AIp
EPd
PIR
ec
1
2/3
4
5
6a
5b
MOp
MOs
scb
ACAd
ACAv

Fig. 8

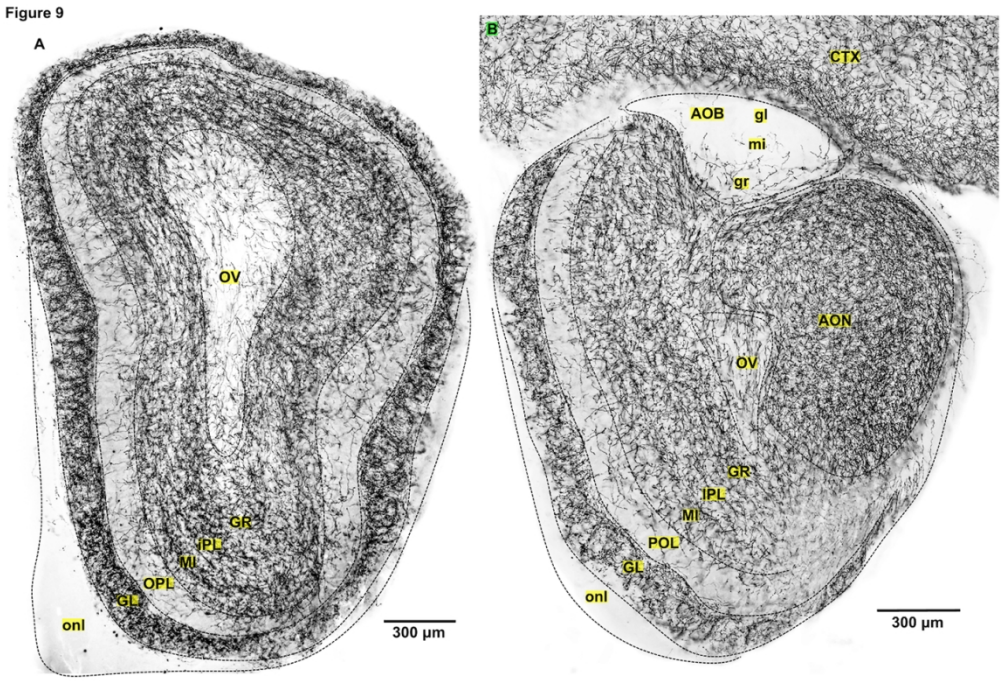
Figure 9
A
OV
GR
IPL
MI
OPL
GL
onl
300 µm
B
CTX
AOB
gl
mi
gr
AON
OV
GR
IPL
MI
POL
GL
onl
300 µm

Fig. 9

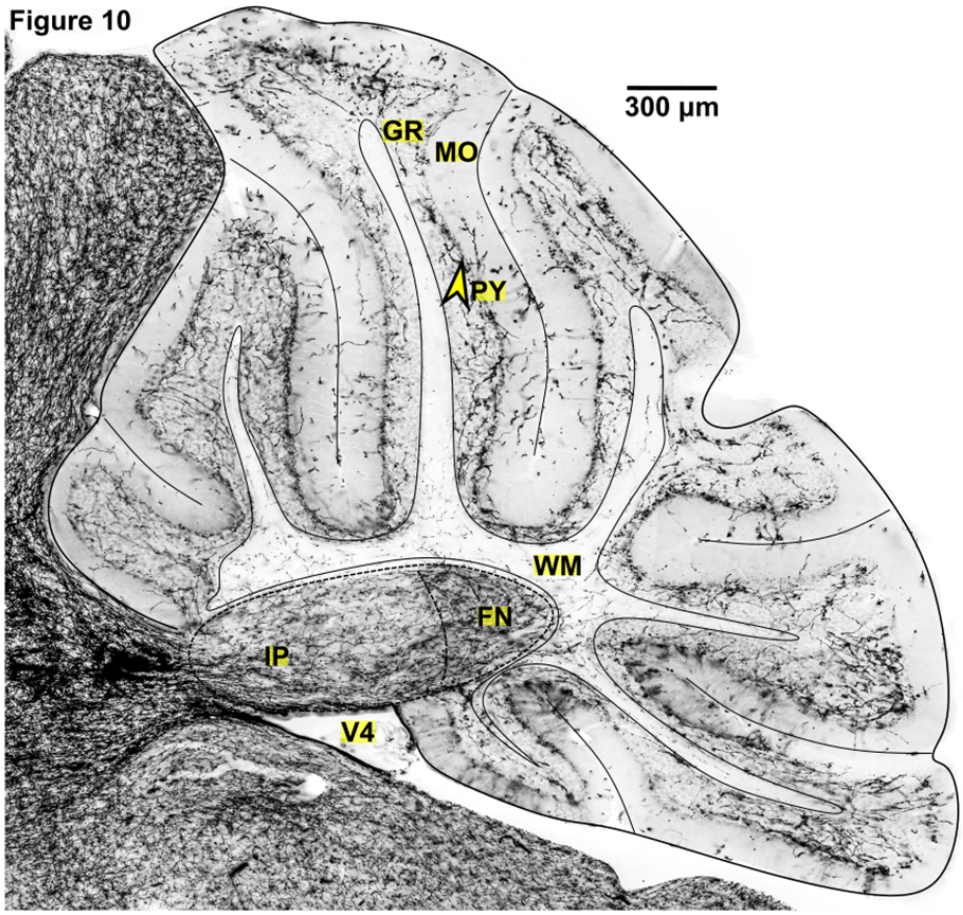

Fig. 10

80x72mm (300 x 300 DPI)